https://doi.org/10.5194/egusphere-2026-3546
Preprint. Discussion started: 7 August 2026
© Author(s) 2026. CC BY 4.0 License.

Exploring drivers of Cloud Condensation Nuclei in the Indian Sector of the Southern Ocean

Sandhya Singh[1], Ashish Soni[1], Shivdas Bankar[1], Ritesh Kumar[2], Rohit Srivastava[2], Sreerag Athirpankandi[2], Rajani Kanta Mishra[2], Jitender Singh[1], Gaddamidi. Sreenivas[1], Amey Datye[1], Yogesh Tiwari[1], Suvarna Fadnavis[1], Thara Prabhakaran[1] and Anoop Sharad Mahajan[1*]

[1] Indian Institute of Tropical Meteorology, Pune, India

[2] National Centre for Polar and Ocean Research, Goa, India

Corresponding author: Anoop Mahajan (anoop@tropmet.res.in)

https://doi.org/10.5194/egusphere-2026-3546
Preprint. Discussion started: 7 August 2026
© Author(s) 2026. CC BY 4.0 License.

Abstract

The Southern Ocean plays a critical role in Earth's climate system, acting as a major sink for heat and carbon dioxide. Clouds over this region strongly influence the regional radiation budget, yet their formation remains poorly understood and represented in climate models. This is partially driven by thHighlightede lack of in-situ observations, particularly over the undersampled Indian sector. In this study, we report on the latitudinal variability of cloud condensation nuclei (CCN) and examine the meteorological and biological factors that can influence their distribution across this region. CCN concentrations were measured during the 12th Indian Scientific Expedition to the Southern Ocean during February and March 2025 aboard a research vessel traversing from 20° S to 68° S. CCN concentrations varied across supersaturation levels, with the highest values approximately 500 cm^{-3} observed at S = 1.0% in the polar band (60-70° S) and lower concentrations at lower S levels. CCN concentrations showed a poor correlation with coarse-mode aerosols, suggesting that wind-driven sea spray does not play a major role in controlling the CCN variability in this region. Chlorophyll a, used as a proxy for biological productivity, showed a positive relationship with CCN concentrations. Air masses passing over biologically productive waters during the preceding 24-48 h were associated with higher CCN concentrations, with the strongest relationship observed within the 30-50° S latitude band encompassing the subtropical and subantarctic fronts. This suggests a closer association between marine biological activity and CCN variability in this region. In contrast, the weaker relationship outside this latitude band indicates that physical processes and non-biological sources may exert a greater influence on CCN concentrations in other regions.

https://doi.org/10.5194/egusphere-2026-3546
Preprint. Discussion started: 7 August 2026
© Author(s) 2026. CC BY 4.0 License.

Introduction

The Southern Ocean has one of the most pristine atmospheres on Earth due to its remote location, away from major populated areas and low continental influence (Hudson et al., 1998; Uetake et al., 2020). It plays a pivotal role in regulating the Earth's climate system by influencing global circulation patterns, carbon cycling, and the global radiative energy budget (Mallet et al., 2023). As a result, it is an ideal place for understanding background processes, which are otherwise difficult to study due to the large signals associated with anthropogenic activities (Carslaw et al., 2013; McCoy et al., 2020). In particular, the Southern Ocean presents a unique test bed for increasing our understanding of aerosol-cloud interactions and the role of marine biogenic aerosols and their precursors (Humphries et al., 2021). Despite this, simulations of clouds, aerosols, and air-sea fluxes in climate and earth system models show significant biases and uncertainties in the Southern Ocean region, driven by a lack of observations (Halfter et al., 2025; McFarquhar et al., 2019; Pierce and Adams, 2009; Shindell et al., 2013).

The Southern Ocean marine environment presents one of the most significant challenges for climate model accuracy, with persistent biases in cloud representation leading to substantial uncertainties in future climate projections (Che et al., 2022). Aerosol-cloud interactions were found to have the largest uncertainty in our understanding of the Earth's climate in the most recent assessments from the Intergovernmental Panel on Climate Change (IPCC, 2023). These model discrepancies in the Southern Ocean result from poor representation of aerosol-cloud interactions, where inadequate parameterisations of cloud condensation nuclei (CCN) formation and activation processes contribute to systematic errors in simulated cloud properties and the resulting radiative forcing (Bodas-Salcedo et al., 2014; Carslaw et al., 2013; Efraim et al., 2020; Niu et al., 2025; Sanchez et al., 2021). Climate models exhibit significant biases in the Southern Ocean, particularly for low-level clouds. Coupled Model Intercomparison Project (CMIP) and Atmospheric Model Intercomparison Project (AMIP) models show shortwave radiation errors linked to poor cloud representation (Hyder et al., 2018). Past studies have shown that mixed-phase cloud processes alone can affect the surface cloud radiative effect in this region (Smith et al., 2025)

Due to the pristine conditions and low anthropogenic impacts observed in the remote marine boundary layer (MBL) within the Southern Ocean, cloud characteristics and radiative forcing are highly sensitive to small changes in aerosol emissions (Downey et al., 1990; Fossum et al.,

https://doi.org/10.5194/egusphere-2026-3546
Preprint. Discussion started: 7 August 2026
© Author(s) 2026. CC BY 4.0 License.

2018; Pierce and Adams, 2006). Most aerosols in this region originate from natural sources, including primary particles such as sea spray produced by wave breaking and bubble bursting, and secondary particles formed through gas-to-particle conversion of biogenic trace gases such as dimethyl sulphide (DMS) (Mallet et al., 2023). Over the Southern Ocean, secondary sulphate is the dominant contributor to CCN number concentration under typical MBL conditions, whereas primary sea-spray contribution varies with wind speed (Fossum et al., 2018; Quinn et al., 2017). Several studies have shown that non-sea-salt sulphate, i.e., from the oxidation of DMS and methane thiol released by phytoplankton and sea ice algae, which leads to the formation of sulphuric acid and methanesulfonic acid (MSA), is the dominant secondary aerosol in this region (Quinn et al., 2000; Sanchez et al., 2018; Wohl et al., 2024).

Trace gases such as DMS and methane thiol play a crucial role in the Southern Ocean (Hulswar et al., 2022; Joge et al., 2024; Manville et al., 2023; Wohl et al., 2024). These volatile sulphur compounds are primarily emitted by marine phytoplankton and undergo oxidation in the atmosphere, producing sulphur-containing compounds, including sulphur dioxide (SO_2) and sulphate aerosols, which contribute to CCN formation (Ayers and Gillett, 2000; de Bruyn et al., 2002; Mace et al., 2023; McCoy et al., 2015). These aerosols influence the Earth's radiation balance directly by scattering solar radiation and indirectly by modifying cloud properties (Charlson et al., 1987; Mahajan et al., 2015). The oxidation pathways of DMS are complex and involve reactions with hydroxyl radicals (OH•) and bromine radicals (Br•), resulting in variability in the production of CCN precursors (Kilgour et al., 2025). The Southern Ocean, with its vast phytoplankton populations, serves as a significant natural source of these trace gases, making an understanding of their atmospheric chemistry essential for climate studies in this region.

CCN serve as a key link between aerosols and cloud microphysics, controlling cloud droplet number concentrations and cloud albedo (Choudhury et al., 2025). In remote ocean regions, CCN concentrations are influenced primarily by marine biological activity, such as emissions of DMS, isoprene, monoterpenes, and their oxidation products, alongside wind-driven sea spray aerosols and entrainment from the free troposphere (Humphries et al., 2023; Mahilang et al., 2021; Zheng et al., 2020). The process of aerosol activation into CCN depends strongly on supersaturation *(S)*, making it necessary to examine CCN across multiple *S* levels to accurately understand cloud formation processes (Svensmark et al., 2024). Variations in trace gases and aerosols profoundly affect cloud albedo and climate feedbacks, as described by the CLAW hypothesis, which proposes a negative feedback loop in which increased DMS emissions from

https://doi.org/10.5194/egusphere-2026-3546
Preprint. Discussion started: 7 August 2026
© Author(s) 2026. CC BY 4.0 License.

phytoplankton enhance CCN production, increasing cloud reflectivity and cooling the climate, which in turn influences biological activity (Charlson et al., 1987). However, recent observations indicate complexities, such as cloud processing of DMS oxidation products, which modulate sulphate aerosol production and CCN availability (Kilgour et al., 2025; Novak et al., 2021; Quinn and Bates, 2011). Overall, wind speed and biological activity influence aerosol production and CCN variability in the Southern Ocean (Mallet et al., 2023), highlighting the need to measure these variables simultaneously in this region.

Existing observational studies have provided important insights into the spatial variability and characteristics of CCN across this region (Humphries et al., 2021; McCoy et al., 2021; Price et al., 2024; Sanchez et al., 2021). Some ship-based campaigns have documented latitudinal gradients in CCN concentrations, showing a transition from mixed continental and marine influences in the northern sectors to predominantly marine biogenic and sea-salt aerosol domination in the southern sectors (Humphries et al., 2021; McCoy et al., 2021). In coastal Antarctica, sulphate-rich air masses have been reported, with CCN activation ranging from 37% to 75% (Fossum et al., 2018). Under typical MBL conditions in the Southern Ocean, sea salt aerosols contribute modestly, but their contribution increases with wind speed, indicating a dynamic interplay between primary sea-spray and secondary sulphate aerosols in marine cloud formation. Hitherto, studies have also shown that CCN variability is influenced not only by local emissions but also by long-range transport and cloud processing (Carslaw et al., 2013; Twohy et al., 2021).

CCN concentrations across the study region are generally low due to its pristine marine environment, but exhibit strong seasonal variability, peaking in summer when biological activity and oceanic emissions increase (Gras, 1990). Korhonen et al. (2008) observed a ~3–fold increase in CCN concentrations during summer, primarily driven by enhanced oceanic biogenic emissions. Model simulations showed that biogenic sources contribute up to ~46% of CCN in mid latitudes and ~40% at higher latitudes. Observations also show that CCN and cloud droplet number concentration correlate with chlorophyll a, a proxy for ocean productivity, highlighting the coupling between ocean biology and CCN formation (McCoy et al., 2015). Recent field campaigns have improved our understanding of CCN variability and new particle formation across the Southern Ocean, but the Indian Sector of the Southern Ocean (ISSO) remains one of the least explored regions, and observations of CCN in this region are scarce (Halfter et al., 2025; McFarquhar et al., 2021; Salim et al., 2023). Existing studies suggest that enhancements in CCN concentrations over the ISSO are linked to biogenic

https://doi.org/10.5194/egusphere-2026-3546
Preprint. Discussion started: 7 August 2026
© Author(s) 2026. CC BY 4.0 License.

emissions (Baccarini et al., 2021; Tatzelt et al., 2022; Tulet et al., 2024). However, the relative contributions and interplay between biological and physical drivers, such as wind-driven sea spray, long-range transport, and biological emissions, remain uncertain (Ayers and Cainey, 2007).

While the role of ocean biological productivity in driving CCN is well established in the Southern Ocean through prior observational and modelling studies, most of this evidence comes from the Atlantic and Pacific sectors. Whether the same mechanisms dominate CCN variability in the Indian sector, how CCN concentrations vary latitudinally across this sector, what the relative contributions of primary sea spray and secondary biogenic aerosol are to CCN number, and what aerosol size characteristics are associated with CCN activity across different latitude bands in this region are questions that remain largely unaddressed due to the scarcity of dedicated in-situ observations from this region. This study aims to investigate CCN variability over the ISSO using a combination of in situ observations, satellite remote sensing data, and back-trajectory analysis during the 12th Indian Scientific Expedition to the Southern Ocean (ISESO-12). We explore CCN variability and its linkage to physical and biological drivers. The observations contribute to a sparse dataset of CCN concentrations in the ISSO and aim to improve the understanding of natural aerosol-cloud interactions in this region.

2 Methods

2.1 Cruise information

Observations were made onboard the research vessel ORV SA Agulhas during the ISOE-12, organised by the National Centre for Polar and Ocean Research (NCPOR) under the Ministry of Earth Sciences (MoES), Government of India. The expedition was conducted during the austral summer/spring, from 11 February to 28 March 2025. The scientific expedition started from Port Louis, Mauritius (20.16° S, 57.50° E), and traversed southward across the subtropical and sub-Antarctic waters of the ISSO, reaching 68° S. The transect included multiple hydrographic and atmospheric sampling stations distributed across distinct oceanic fronts, including the Subtropical Front (STF), Subantarctic Front (SAF), and Polar Front (PF), before returning to Mauritius along the 57.5° E longitude line. The cruise traversed diverse oceanic regimes, from biologically productive frontal zones to pristine polar waters, allowing examination of spatial gradients (Fig. 1). In addition to the in situ measurements collected during the expedition, meteorological reanalysis and satellite observations were used to support the analyses. A summary of all datasets used in this study is provided in Table 1.

https://doi.org/10.5194/egusphere-2026-3546
Preprint. Discussion started: 7 August 2026
© Author(s) 2026. CC BY 4.0 License.

2.2 Meteorological parameters

Multiple meteorological parameters were continuously monitored using an automatic weather station (AWS) installed on the monkey deck of R/V SA Agulhas during ISESO-12. The AWS used was the Lufft WS600 Smart Weather Sensor, interfaced with a Campbell Scientific CR1000X datalogger. The WS600 employs ultrasonic technology to simultaneously measure wind speed (accuracy ±0.3 m s^{-1} or ±3% in the range 0-35 m s^{-1}, and ±5% above 35 m s^{-1}), wind direction (RMSE < 3° at wind speeds above 1.0 m s^{-1}), air temperature (±0.2°C in the range -20 to +50°C, and ±0.5°C above -30°C), relative humidity (±2% RH), and precipitation intensity (±0.2°C under laboratory conditions). Calibration of the AWS was performed before and after the cruise, and no significant difference was observed between the two. Data were recorded at 1-second intervals and archived by the CR1000X.

2.3 Back-trajectory analysis

To study the origin of the air masses sampled during the expedition, 5-day (120-hour) back-trajectories were calculated using the NOAA HYSPLIT (Hybrid Single-Particle Lagrangian Integrated Trajectory) model (Draxler et al., 1999). Trajectories were calculated every 6 hours along the cruise track at an arrival height of 100 m. The model used the Global Data Assimilation System (GDAS) meteorological dataset with a 1.0° x 1.0° spatial resolution. Fig. 1 shows the cruise track and the 5-day air mass back-trajectories along the ship track.

The back trajectories confirm that the air masses sampled during the cruise were predominantly of marine origin, arriving from the west and southwest under the influence of the prevailing Southern Ocean westerlies. This circulation regime, the so-called “Roaring Forties” and “Furious Fifties”, is characteristic of the Southern Hemisphere mid-latitude. Very few trajectories originate from northerly directions, i.e., from continental or tropical regions, confirming the predominantly pristine marine character of the sampled air. This low terrestrial influence is an essential prerequisite for studying natural marine aerosol-CCN production mechanisms without anthropogenic signals and validates the use of these measurements to investigate biogenic and sea-spray CCN sources in isolation.

2.4 Black carbon observations

Black carbon (BC) mass concentrations were measured using an aethalometer (AE33, Magee Scientific, USA). The aethalometer uses dual-spot technology to minimise artefacts in BC

https://doi.org/10.5194/egusphere-2026-3546
Preprint. Discussion started: 7 August 2026
© Author(s) 2026. CC BY 4.0 License.

measurements over filter substrate using optical methods. The attenuation of light due to aerosol deposition on the filter was measured at seven wavelengths (370, 470, 520, 590, 660, 880, and 950 nm) with a temporal resolution of 1 minute. Since BC exhibits maximum absorbance at 880 nm (Drinovec et al., 2015), the attenuation measured at this wavelength was used for the derivation of BC mass concentration. A Mass Absorption Cross-section (MAC) value of 7.77 $m^2\ g^{-1}$ at 880 nm, recommended for pristine environments and consistent with the manufacturer's recommendation, was used in this study (Singh et al., 2024). Direct measurements of BC using an Aethalometer over oceanic regions can be affected by high relative humidity, introducing uncertainties due to hygroscopic growth and changes in aerosol optical properties. To minimise these effects, a sample stream dryer (Magee Scientific) was used to maintain RH below 40%, as recommended by the World Meteorological Organisation (WMO) (Wiedensohler et al., 2013). The Aethalometer was calibrated before the expedition. BC mass concentration was considered a key parameter for identifying and filtering contaminated data associated with ship exhaust emissions. The instrument was installed alongside other in situ instruments in an atmospheric laboratory located on the forward side of the ship's first deck, opposite to the exhaust outlet, and connected to the inlet through a 3 m long static-dissipative flexible sampling tube.

2.5 Cloud condensation nuclei measurements

CCN concentrations were measured using a dual-column cloud condensation nuclei (CCN) counter (CCN-200, Droplet Measurement Technologies, USA). (Droplet Measurement Technologies, 2017; Roberts & Nenes, 2005). Aerosol particles were activated under predefined supersaturation conditions within the columns, enabling CCN observations. The activated particles were counted at the end of the column using an optical particle counter in 20 size-resolved bins from 0.75 to 10 µm. The CCN counter was located on the first deck, with a 3 m inlet length. A Nafion dryer was installed between the inlet tube and the CCN counter to maintain relative humidity (RH) below 40%. One column was set to count CCN at a fixed supersaturation of 0.4%, while the second column cycled between different supersaturation ranges (0.2%, 0.4%, 0.6%, 0.8%, and 1.0%). The column was operated for 10 minutes at 0.2% supersaturation, followed by 5 minutes at each of the remaining supersaturation settings. The complete measurement cycle lasted 30 minutes. Only data points corresponding to periods when the set-point temperatures had stabilised were initially retained. To minimise the influence of unstable operating conditions, the first 3.5 minutes and the last 30 seconds of each supersaturation cycle were excluded from the analysis due to high noise. The inlet was cleaned

https://doi.org/10.5194/egusphere-2026-3546
Preprint. Discussion started: 7 August 2026
© Author(s) 2026. CC BY 4.0 License.

with particle-free zero air daily to remove any unwanted sea spray residue. Before the campaign, comprehensive pre-deployment checks were conducted to ensure the reliability of CCN measurements. The CCN counter underwent sample and sheath flow calibrations using a Gilibrator volumetric flow meter as the calibrated reference. The calibration coefficients (slope and intercept) for the sample and sheath flows of both columns were updated in the instrument software to correct the measured flow rates, ensuring the prescribed total flow and stable supersaturation conditions throughout the measurements. The calibration coefficients for sample and sheath flow were determined separately for both columns and updated in the instrument software (Column A: sample slope = 57.52, intercept = -129.09; sheath slope = -592.94, intercept = 1345.73; Column B: sample slope = 60.69, intercept = -135.56; sheath slope = -570.04, intercept = 1313.33). The Optical Particle Counter performance was evaluated through a diameter verification test using a monodisperse aerosol generator, allowing assessment of particle sizing accuracy and overall instrument health. In addition, a zero-filter test was performed by installing a High-Efficiency Particulate Air filter at the inlet to confirm near-zero particle counts and ensure no internal contamination or electronic noise. These procedures established a robust baseline for instrument performance prior to the field campaign.

To ensure that the CCN data were free of ship-stack contamination, a detailed quality-control procedure was followed. The exhaust plume from the ship can occasionally affect measurements when the wind is from the direction of the ship's stack. To reduce this contamination, data were analysed only when the wind direction was between 315° and 45° relative to the ship's bow, as the likelihood of the air mass being influenced by the ship's stack increases in other directions. Next, periods with low ambient relative wind speeds (< 4 m s^{-1}) were excluded because, under such calm conditions, the dispersion of exhaust gases is limited and pollutants can be advected near the sampling inlet by small eddies. Finally, the ship's steaming speed was also used to filter out stationary measurements, as these periods are highly likely to be contaminated. In addition to these meteorological filters, the data were screened using BC concentrations as an indicator of combustion influence, considering the clean background and the absence of other point sources. An absolute threshold of 600 ng m^{-3} was applied to the raw BC time series values. Exceeding this threshold, events were flagged as ship exhaust contamination events. The interquartile range (IQR) method was applied to the remaining BC data, with values exceeding Q3 + 1.5 × IQR flagged as residual outliers. Lastly, a visual inspection of the time series was performed to identify any remaining anomalous

https://doi.org/10.5194/egusphere-2026-3546
Preprint. Discussion started: 7 August 2026
© Author(s) 2026. CC BY 4.0 License.

spikes not captured by the automated criteria. CCN measurements corresponding to all flagged periods across these steps were excluded from further analysis. After applying these filters, only measurements that met all the criteria above were retained. Thus, the CCN concentrations used for further analysis reflect natural aerosol populations rather than ship-related contamination.

To examine the dependence of CCN concentration on supersaturation, the measured CCN concentrations at the five supersaturation levels (S = 0.2%, 0.4%, 0.6%, 0.8%, and 1.0%) were fitted using the Twomey power-law relationship. The power-law exponent k was derived by fitting the CCN concentrations measured at five supersaturation levels to the Twomey power-law equation (Eq. 1) (Twomey, 1959)

$$N_{CCN} = C.SS^{k} \quad (1)$$

where N is the CCN concentration at supersaturation S, C is a scaling constant, and k is the exponent describing the sensitivity of CCN concentration to supersaturation.

2.6 Aerodynamic particle sizer measurement

Aerosol number concentrations were measured using an Aerodynamic Particle Sizer (APS, 3321, TSI, USA). Throughout the observation period, the APS aerosol and sheath flow rates were maintained at 1 and 4 L min^{-1}, respectively. The APS was calibrated before the expedition to ensure high measurement accuracy. APS determines the size of aerosol particles based on the time of flight of the particles between two laser beams. Due to their greater inertia, larger particles accelerate more slowly than smaller particles, allowing the instrument to classify particles by aerodynamic size. This instrument provides real-time aerosol number concentration in size bins ranging from 0.5 µm to 20 µm. An intercomparison experiment involving 15 APS instruments of the same model reported an uncertainty of approximately 10% in particle sizing accuracy relative to polystyrene latex standard particles (Pfeifer et al., 2016). The instrument was installed alongside other in situ instruments in a laboratory located on the forward section of the ship's first deck to minimise potential contamination from ship exhaust emissions and was connected through a 3 m long conductive silicone sampling tube with an inner diameter of 1.73 cm. In the present study, aerosol concentration data were collected at a 5 min temporal resolution. Filters similar to those for CCN were applied to the APS measurements.

2.7 Exposure calculations

https://doi.org/10.5194/egusphere-2026-3546
Preprint. Discussion started: 7 August 2026
© Author(s) 2026. CC BY 4.0 License.

To explore the environmental drivers of CCN variability, exposure-based analyses were performed along the computed back trajectories. Daily chlorophyll a data from the Copernicus GlobColour satellite, spatial resolution: 0.042° x 0.042°, ≈ 4.6 km (Mansour et al., 2023) were used as a proxy for phytoplankton biomass and marine biogenic emissions. Satellite-derived chlorophyll a provides gap-free daily global composites through a weighted merging of multiple satellite sensors, including MODIS-Aqua (Moderate Resolution Imaging Spectroradiometer on NASA's Aqua satellite), VIIRS (Visible Infrared Imaging Radiometer Suite), and OLCI (Ocean and Land Colour Instrument on ESA's Sentinel-3 satellites). The gap-free nature of this product addresses the temporal sampling uncertainty associated with cloud cover, which is a well-known limitation of single-sensor satellite retrievals over the frequently cloudy Southern Ocean. These were validated using the in situ surface chlorophyll a concentration along the cruise track from 0 m seawater samples using an Agilent 1260 Infinity HPLC system equipped with a C8 column (4.6 x 150 mm, 3.5 µm particle size) and a diode array detector at 450 and 665 nm (Heukelem and Thomas, 2001). Of particular interest is the emission sensitivity near the surface, which can be used as an indicator of sea-air emissions. To measure the surface influence of biogenic emissions, the chlorophyll a value along each trajectory was integrated at each time step over the 5-day period when the air mass remained within the MBL (1000 m).

Similarly, the wind speed effect along the trajectory (as it affects the sea-air exchange) was estimated using ERA5 reanalysis data at the 10 m level. For each air mass back-trajectory, wind speed values were extracted at the corresponding positions for each time step. These values were then integrated along the trajectory to obtain the total wind speed effect experienced by the air mass. This integrated wind speed indicates the extent to which surface winds may have contributed to aerosol generation along the back trajectory history.

2.8 Cloud droplet number concentrations retrieval

Cloud droplet number concentrations (N_d) along the cruise track were retrieved using the MODIS/Terra Level 2 cloud products (MOD06_L2), i.e. cloud optical thickness (COT) and cloud effective radius (CER). Shipboard observations were temporally matched with MODIS overpasses using hourly-averaged measurements corresponding to the satellite overpass time. Spatial collocation was performed using a nearest-neighbour approach, retaining only MODIS pixels within 0.1° of the ship's position to ensure consistency between satellite and in situ

https://doi.org/10.5194/egusphere-2026-3546
Preprint. Discussion started: 7 August 2026
© Author(s) 2026. CC BY 4.0 License.

observations. N_d was then calculated following the equation (Grosvenor et al., 2018) using MODIS-derived COT and CER:

$$N_d = \frac{\sqrt{5}}{2\pi k} \times \sqrt{\frac{f_{ad} \times c_w \times COT}{Q_{ext} \times \rho_w \times CER^5}} \quad (2)$$

where:

where N_d is the cloud droplet number concentration, f_{ad} is the adiabatic fraction (1), c_w is the water content coefficient (2.3×10^{-6} kg m^{-4}), COT is the MODIS-derived cloud optical thickness, Q_{ext} is the extinction efficiency (2.0), ρ_w is the density of water (1000 kg m^{-3}), CER is the MODIS-derived cloud effective radius (m), and k is the constant dispersion parameter (0.8).

It is worth noting that estimating N_d from satellite data may introduce systematic errors due to several assumptions about cloud parameters (Gryspeerdt et al., 2022). The main rationale for using N_d is not to present the absolute value, but rather to show its relationship with CCN counts.

3 Results and Discussion

3.1 CCN temporal variability

CCN concentrations exhibited considerable variability across all supersaturation (S) levels throughout the expedition. Observed values ranged from 9-347 cm^{-3} at S = 0.2%, 13-485 cm^{-3} at S = 0.4%, 15-486 cm^{-3} at S = 0.6%, 14-499 cm^{-3} at S = 0.8%, and 12-500 cm^{-3} at S = 1.0%. As expected, the upper limit of CCN concentrations increased progressively with higher supersaturation, indicating that a larger fraction of the ambient aerosol population was activated at higher supersaturation levels. These concentrations are consistent with prior ship-based observations in the Southern Ocean. Sanchez et al. (2021) reported CCN concentrations between 100-300 cm^{-3} at S = 30% during the Southern Ocean Clouds, Radiation Aerosol Transport Experimental Study (SOCRATES) campaign south of Australia. Our observations at S = 0.2% generally fall within the reported range and are broadly consistent with it. Fossum et al. (2018) found CCN concentrations in the range of 300 to 400 cm^{-3} in the Atlantic sector of the Southern Ocean. Schmale et al. (2019) reported regionally varying CCN concentrations across multiple Southern Ocean sectors at S = 0.2%, with concentrations in the same range as our observations in the ISSO. Humphries et al. (2021) reported a clear latitudinal gradient in

https://doi.org/10.5194/egusphere-2026-3546
Preprint. Discussion started: 7 August 2026
© Author(s) 2026. CC BY 4.0 License.

CCN across the Southern Ocean at S = 0.2% and 50%, with concentrations increasing from the mid-latitudes toward the southern sector. Our observations at S = 0.2% agree well with their reported values. Similarly, Niu et al. (2024), based on the Measurement of Aerosols, Radiation, and Clouds over the Southern Ocean (MARCUS) campaign observations (50° S-68° S) at S = 0.2% and 50%, found strong seasonal and latitudinal variability, with enhanced CCN over the summer in the Southern Ocean (62° S-68° S), which are also consistent with the polar enhancement observed in our dataset.

The time series at supersaturations of 0.2%, 0.4%, 0.6%, 0.8%, and 1.0% (Fig. 2) shows a coherent temporal pattern throughout the expedition, with peaks and troughs occurring nearly simultaneously across all five channels, suggesting that the aerosol population responded to the same atmospheric forcing rather than to independent changes in individual size classes. This co-variability indicates control by common drivers such as air mass origin, sources, and wind conditions, with a pronounced episode of elevated concentrations in late February and a sustained low period in mid-March. CCN concentrations are the lowest at S = 0.2%, as only the largest and most hygroscopic particles are activated at this low supersaturation. As supersaturation increases from 0.2% to 1.0%, CCN concentrations increase progressively as higher supersaturation activates progressively smaller, less hygroscopic particles. This behaviour is consistent with the Köhler theory (Köhler, 1936) which describes how aerosols can activate into cloud droplets depending on their size and chemical composition. The concurrent rise and fall across all five S levels suggests that the aerosol populations within the study area during this expedition were relatively uniform and broadly distributed across sizes, rather than concentrated in a narrow size range, consistent with previous studies highlighting coherent CCN activation behaviour (Bougiatioti et al., 2011; Dusek et al., 2006.; Paramonov et al., 2015).

3.2 Latitudinal distribution of cloud condensation nuclei and chlorophyll a along the ship track

The spatial distribution of daily mean CCN concentrations along the ship track shows a clear latitudinal variability, with relatively higher values observed close to coastal Antarctica (Fig. 3a). The highest daily mean CCN concentrations are seen in the sub-Antarctic zone between 55° S and 60° (averaging ~300 cm^{-3}). Lower concentrations (75-110 cm^{-3}) are observed over subtropical latitudes (20° S-30° S) and at some higher polar locations, where continental air masses arrived from the Antarctic continent or from the sea-ice zone with limited oceanic

https://doi.org/10.5194/egusphere-2026-3546
Preprint. Discussion started: 7 August 2026
© Author(s) 2026. CC BY 4.0 License.

exposure. However, the highest concentrations were also observed close to the Antarctic coast. The elevated CCN concentrations at higher polar latitudes mirror previous cruises in the Southern Ocean (Humphries et al., 2021; Humphries, et al., 2023; Niu et al., 2024)

Satellite-derived chlorophyll a along the ship track also reveals a pronounced latitudinal gradient (Fig. 3b). Oligotrophic subtropical gyre waters (20° S-35° S) are characterised by very low chlorophyll a (<0.05 mg m^{-3}), while biologically productive sub-Antarctic waters (approximately 40° S-45° S) and near-Antarctic coastal waters (60-65° S) display elevated chlorophyll a value of 0.2-0.4 mg m^{-3}. The close spatial link between surface productivity (chlorophyll a) and CCN suggests that regions with higher biological activity also tend to have more cloud-forming particles, consistent with patterns observed across the Southern Ocean (Mace et al., 2023; McCoy et al., 2015; Twohy et al., 2021). This is because biologically productive frontal zones release volatile compounds and organic matter that act as important precursors for cloud-active aerosols (Saliba et al., 2020).

3.3 Latitudinal gradients in cloud condensation nuclei concentration and supersaturation dependence

The latitudinal distribution of CCN is discussed in this section. At the lowest supersaturation (S = 0.2%), CCN concentrations are lowest in the 20-30° S latitude band (mean: 105 cm^{-3}, median:112 cm^{-3}) refer Table 2, reflecting the homogeneous, aerosol-sparse character of the oligotrophic subtropical gyre where limited phytoplankton productivity restricts biogenic aerosol precursor supply (Fig. 3d). The mean and median CCN concentrations increase modestly in the polar band (60-70° S) at S = 0.2% (mean: 175 cm^{-3}; median: 181 cm^{-3}). As supersaturation increases from 0.2% to 1.0%, the mean and median CCN concentrations rise systematically across all latitude bands. The polar band shows an increase from 175 cm^{-3} at S = 0.2% to 326 cm^{-3} at S = 1.0% (the median rises from 181 to 323 cm^{-3}). The polar band consistently recorded the highest mean and median CCN concentrations across all supersaturation levels. The systematic amplification of CCN with increasing supersaturation implies that the MBL contains a substantial population of small, lower hygroscopic particles that can act as CCN only at higher supersaturations. This is further supported by the power-law exponent k (Fig. 3c), which shows the lowest values (k = 0.38-0.40) in the Polar band and the highest values ($k \approx 0.59$) in the subtropical band (20-30° S), indicating that polar aerosols activate less efficiently at intermediate S, but contribute increasingly at higher S levels.

https://doi.org/10.5194/egusphere-2026-3546
Preprint. Discussion started: 7 August 2026
© Author(s) 2026. CC BY 4.0 License.

These particles likely include freshly nucleated biogenic sulphate in early growth stages near the sea-ice edge (Charlson et al., 1987) or iodine oxide clusters in areas where biological activity within sea ice drives iodine emissions directly into the coastal Antarctic atmosphere (Saiz-Lopez et al., 2015), providing the precursor supply for new particle formation events documented in polar and coastal Antarctic regions (Jokinen et al., 2018; Sipilä et al., 2016). Algae additionally produce organic compounds that can contribute to primary and secondary marine aerosol, with hygroscopicity distinct from open-ocean sulphate (Lizotte, 2001), further enriching the polar boundary layer with particles that reveal their full CCN potential only under the highest supersaturation levels.

Fig. 3c also reflects the day-to-day variability in aerosol loading within each latitude band. At $S = 0.2\%$, the standard deviation (SD) was relatively small, ranging from 48 cm^{-3} in the 30-40° S band to 73 cm^{-3} in the 40-50° S band, indicating stable and consistent conditions. At $S = 1.0\%$, however, the SD increased substantially to 118 cm^{-3} in the 50-60° S band and 115 cm^{-3} in the 40-50° S band, reflecting the episodic nature of the tiny particles that activate only at high supersaturation. This suggests that particles most likely form new particle formation events, which occur only when atmospheric conditions are favourable, i.e. sufficient precursor gases, adequate OH• to oxidise them, and a low condensation sink.

3.4 Wind speed and cloud condensation nuclei

To assess the role of wind-driven sea-spray production as a CCN source, we checked the correlation between CCN concentrations and wind speed integrated along the HYSPLIT back-trajectories at three lookback periods: 24, 48, and 120 hours (Fig. 4). At the shortest lookback time of 24 hours (Fig. 4a), the correlations were weak, with Pearson's r values ranging from -0.05 to +0.05 across all S levels, and none were statistically significant ($p > 0.05$). This shows that the wind speed experienced by the air mass over the last 24 hours did not heavily influence the CCN concentrations. As the trajectory lookback extended to 48 hours (Fig. 4b), a statistically significant negative correlation appeared at $S = 1.0\%$ ($r = -0.26$, $p = 0.006$), with weaker non-significant trends at other S levels. By 120 hours (Fig. 4c), a negative correlation is observed across all S levels and is significant at 95% or better, consistent with the anticorrelation between wind speed and CCN reported in the Southern Ocean by Vallina et al. (2006). This paradoxical observation, in which faster transport delivers fewer CCN, has been theoretically described by Fossum et al. (2018) and Korhonen et al. (2008). They suggest that higher wind speeds lead to less exposure of the air mass to surface emissions of CCN

https://doi.org/10.5194/egusphere-2026-3546
Preprint. Discussion started: 7 August 2026
© Author(s) 2026. CC BY 4.0 License.

precursors, such as DMS, and hence to lower CCN concentrations. The fact that the effect is strongest at S = 1.0%, the channel most sensitive to small, freshly formed particles, provides further support to the idea that fast air masses not only accumulate fewer volatile compounds emitted by the ocean but also allow less time for new particles to grow from the nucleation mode into CCN-active accumulation mode sizes. The weak correlation with wind speed, paired with the relationship observed with chlorophyll a, indicates that biological and chemical processes likely played a more dominant role in CCN production than mechanical wind generation during this cruise, aligning with past reports (Sanchez et al., 2018; Tatzelt et al., 2022).

The in-situ wind speed measured on the ship, however, shows a positive correlation (significant at 95%) with S between 0.2% and 0.4%, whereas correlations are not significant at higher S values (Fig. 5a). This positive correlation at lower S suggests the immediate, local production of sea-spray aerosols, with stronger winds generating larger and more frequent breaking waves that eject more sea-salt droplets into the MBL (Fossum et al. 2018). Sea salt particles are large and highly hygroscopic, activating preferentially at low supersaturation. The fact that the correlation fades at higher S levels indicates that local sea spray predominantly contributes to the large particles that are readily activated, whereas the high-S channels remain dominated by biogenic submicron aerosols that are less sensitive to local winds. The simultaneous negative correlation with trajectory-based wind speed and positive correlation with local wind speed are not contradictory, as they reflect two distinct aerosol production mechanisms operating at different timescales. Local wind governs sea spray (timescale: seconds to minutes), while trajectory wind governs biogenic emissions (timescale: 1-4 days). Together, the two sources explain the observed CCN spectrum.

Quinn et al. (2017) stated that sea spray generally contributes less than 30% to the total CCN population outside of high southern latitudes. High-wind events can exponentially boost primary sea salt emissions, directly injecting larger accumulation-mode particles into the atmosphere (McFarquhar et al., 2021; Tatzelt et al., 2022). This effect is particularly pronounced near the sea-ice zone and coastal Antarctica, where strong winds trigger blowing snow or open local polynyas, mechanically generating highly active sea-salt CCN (Tatzelt et al., 2022).

The wind-speed analysis showed that local winds contribute to CCN formation through sea-spray production. To further investigate this, CCN concentrations were compared with

https://doi.org/10.5194/egusphere-2026-3546
Preprint. Discussion started: 7 August 2026
© Author(s) 2026. CC BY 4.0 License.

simultaneous APS measurements, which capture coarse-mode particles (0.5-20 µm) dominated by sea-salt aerosol. Fig. 6 shows that the correlation between APS measurements and CCN was weakly positive but significant across all S levels, $r = 0.16$ ($p < 0.01$) at $S = 0.2\%$ and $r = 0.17$ ($p < 0.01$) at $S = 1.0\%$. A slightly stronger, but still modest positive correlation, was observed at $S = 0.6\%$ ($r = 0.28$; $p < 0.01$) and $S = 0.8\%$ ($r = 0.23$; $p < 0.01$). APS gives an estimate of the abundance of coarse-mode particles relative to the observed CCN population. To quantify this relationship, the ratio of APS total particle concentration to CCN concentration was calculated for each supersaturation level. The median APS/CCN concentration ratio decreased from 3.83% at $S = 0.2\%$ to 1.58% at $S = 1.0\%$, with corresponding mean ratios ranging from 6.62% to 2.63%. These low ratios indicate that the measured coarse-mode particle concentration constituted only a small proportion of the observed CCN concentration. However, because the APS does not distinguish between CCN-active and CCN-inactive particles and does not measure particles smaller than 0.5 µm, these ratios should not be interpreted as the actual fraction of CCN originating from coarse-mode particles. Instead, they provide an upper-bound indication of the relative abundance of coarse-mode particles compared with the total CCN population. The large gap between consistently low APS counts and highly variable CCN concentrations across all S levels shows that the dominant CCN population resides in the submicron size range, below the APS detection limit, and is most likely of secondary marine aerosol origin, consistent with biogenic emissions, for example, through volatile sulphur compound oxidation, as discussed above.

3.5 Biological signal in cloud condensation nuclei

Before exploring how ocean biology influences CCN, it is important to verify that the satellite chlorophyll a product used in this analysis accurately reflects the biological conditions encountered during the expedition. Fig. 5b shows the correlation between daily satellite-derived chlorophyll a and in situ chlorophyll a measurements collected along the ship track. A significant positive correlation was found ($r = 0.60$; $p = 0.02$), indicating that the satellite product broadly captures phytoplankton biomass patterns along the transect, despite the well-known challenges of satellite retrieval in the high-latitude, frequently cloudy Southern Ocean. We use chlorophyll a exposure analysis to assess direct evidence for links between ocean biological productivity and CCN concentrations. Satellite-derived chlorophyll a encountered by each air mass along its trajectory was summed over 24, 48, and 120 hours, and the chlorophyll a exposure correlations against measured CCN concentrations at all five supersaturation levels were studied (Fig. 7). At 24-hours (Fig. 7a), positive correlations were

https://doi.org/10.5194/egusphere-2026-3546
Preprint. Discussion started: 7 August 2026
© Author(s) 2026. CC BY 4.0 License.

found across all S levels, with the strongest signal at S = 0.2% (r = 0.45; p < 0.01), followed by S = 0.4% (r = 0.37; p < 0.01), S = 0.6% (r = 0.29; p < 0.01), S = 1.0% (r = +0.29; p < 0.01), and S = 0.8% (r = 0.25; p < 0.01). For the 48-hour (Fig. 7b) back trajectories, the correlations remained similarly significant, with S = 0.2% (r = 0.40; p < 0.01) and S = 0.4% at (r = 0.39; p < 0.01), indicating that air masses passing over biologically productive waters in the preceding 24–48 hours could carry more biogenic aerosol precursors, resulting in higher CCN concentrations. The elevated CCN concentrations in this region are likely driven by high biological productivity, which aligns with observations by Humphries et al. (2016), who noted increased secondary aerosol formation associated with biological activity.

To further investigate which latitude bands show the largest chlorophyll a exposure-CCN relationship, latitude-resolved correlation heatmaps were computed for each exposure time and supersaturation level (Fig. 8). For the 24-hour trajectories (Fig. 8a), the 30-40° S band showed the strongest positive correlations across all S levels, with the highest correlation observed at S = 0.4%. Significant positive values persisted across all five supersaturation levels. The 40-50° S band also showed a positive contribution for the 24-hour back trajectories, particularly at higher S levels (S = 1.0%), suggesting that in this band the biological signal is clearer in the smaller particle population. For the 48-hour trajectories (Fig 8b), both the 30-40° S and 40-50° S bands showed consistent positive correlations, while the 50-60° S band showed a stronger correlation at S = 0.2%, indicating limited biological contribution restricted to the larger hygroscopic particle population. Overall, the relationship was strongest at lower and mid-latitudes (30-50° S), coinciding with the subtropical and subantarctic fronts. Emerging as the primary zone where ocean biological productivity drives CCN concentrations, consistent with the high phytoplankton productivity characteristic of these frontal regions. Past observations of CCN precursors also show this effect (Andreae et al., 1995; Ayers and Gras, 1991; Hegg et al., 1991; Korhonen et al., 2008; Lana et al., 2012; Sanchez et al., 2018). While data from the polar band (Fig. 7c) showed greater scatter, likely reflecting additional CCN sources such as sea-ice biological emissions, iodine-driven new particle formation (Atkinson et al., 2012; Inamdar et al., 2020; Mahajan et al., 2021; Roscoe et al., 2015), or continental air masses from the Antarctic, not captured by the chlorophyll a metric. In the case of the 120-hour back trajectories, the correlations weakened substantially across all S levels and are mostly not significant at 95%, suggesting that the biological imprint on CCN becomes less distinct over longer transport timescales due to mixing, wet deposition, and chemical transformation of the original precursor signal (Korhonen et al., 2008).

https://doi.org/10.5194/egusphere-2026-3546
Preprint. Discussion started: 7 August 2026
© Author(s) 2026. CC BY 4.0 License.

The dependence of the chlorophyll a-CCN relationship on supersaturation provides further physical insight. For the 24- and 48-hour trajectories, the positive relationship was stronger at lower supersaturations (S = 0.2% and 0.4%), indicating that biologically sourced particles preferentially contribute to the larger, more hygroscopic accumulation-mode CCN population that activates at low S. At higher supersaturations (S = 0.8% and 1.0%), the correlations weakened somewhat, consistent with a larger, more diverse fraction of particles activating at high S, which dilutes the specific biological signal. It also suggests that local emissions of CCN precursors do not contribute heavily to the CCN signal, suggesting that atmospheric transformation over 24-48 hours are needed for the precursors to grow into CCN. At 120-hour exposure, the relationship was weak across all supersaturations, confirming that the influence of biological productivity becomes indistinct beyond approximately five days of atmospheric transport. These findings are consistent with Vallina et al. (2006), who, using satellite data, demonstrated that chlorophyll a is the dominant control on CCN variability in the Southern Ocean via the DMS oxidation pathway. While their analysis operated at seasonal timescales, our trajectory-based chlorophyll a exposure metric resolves this biological imprint at a 24 to 120-hour scale. The observed relationship between CCN and biogenic emission precursors indicates an important contribution of biogenic emissions to CCN production (Twohy et al. (2021).

3.6 Relationship between cloud droplet number concentration and cloud condensation nuclei

Analysis showed that the 30-50° S band exhibits the strongest link and the most consistent positive chlorophyll a-CCN relationship. To determine whether this biological influence on CCN translates into a measurable change in cloud droplets, CCN concentrations were correlated with cloud droplet number concentrations (N_d) across the transect at all five supersaturation levels. In the 30-50° S band, CCN and N_d are positively and significantly correlated at S = 0.2% (r = 0.56, $p < 0.05$), at S = 0.4% (r = 0.61, $p < 0.05$), at S = 0.6% (r = 0.57, $p < 0.05$), and at S = 0.8% (r = 0.53, $p < 0.05$). The correlation was not significant at S = 1.0%. This pattern aligns with how Nd is generally known to respond to CCN, i.e., more CCN leads to more droplets, only when droplet number is limited by the number of available particles, not when it is limited by updraft strength or supersaturation in the cloud (Rosenfeld et al., 2014). Notably, the 30-50° S band showed both the strongest chlorophyll a-CCN relationship and a clear increase in cloud droplet number concentrations with CCN, consistent with the classic Twomey response (Twomey, 1977). A similar relationship was observed during

https://doi.org/10.5194/egusphere-2026-3546
Preprint. Discussion started: 7 August 2026
© Author(s) 2026. CC BY 4.0 License.

the Indian Ocean Experiment (INDOEX), where Hudson and Yum (2002) found a linear relationship between cloud droplet and CCN concentrations.

Outside this latitudinal band, the correlation between CCN and N_d is weak and not significant at any *S* level. The lack of a significant CCN-N_d relation suggests that there is another variable overriding the expected signal and that N_d is not controlled by CCN alone (Kang et al., 2022; Mace et al., 2021; McFarquhar et al., 2021; Mcfarquhar et al., 2022.; Muhlbauer et al., 2010; Smith et al., 2025; Zheng et al., 2024). Indeed, past Southern Ocean campaigns such as MARCUS and CAPRICORN have shown that mixed-phase clouds, common at higher latitudes, are strongly affected by ice processes and precipitation, which can control droplet number regardless of CCN (McFarquhar et al., 2021). Cloud droplet numbers have also been shown to decrease as air masses travel over the ocean due to the washing out of droplets (Wood et al., 2012), which can break the link between collocated observations of CCN and N_d. In the subtropical band, aerosol levels are already high (as seen in the APS measurements), so adding more CCN makes little difference to droplet number.

4 Conclusions

The Indian sector of the Southern Ocean is undersampled, limiting understanding of aerosol-cloud interactions. The CCN measurements collected from 20°S to 68°S during the austral late summer of February-March 2025 provide a valuable dataset and reveal clear meridional contrasts in CCN sources and behaviour. CCN concentrations showed a systematic poleward increase across all five supersaturation levels, with the lowest values in the oligotrophic subtropical band and the highest in the polar band, reflecting fundamental differences in aerosol sources, composition, and processing across the latitudinal transect.

The comparison between CCN and coarse-mode aerosol measurements confirmed that wind-driven sea spray is not the dominant source of CCN number concentration in this region, with the dominant CCN population residing in the sub-micron accumulation mode. CCN variability was jointly shaped by ocean biological productivity, air mass transport history, and local wind-driven sea-spray production. Trajectory-integrated wind speed showed a negative relationship with CCN at longer times, consistent with faster air mass transport reducing ocean surface residence time and limiting biogenic aerosol precursor accumulation, while local wind speed showed a positive contribution at low supersaturation through sea-spray production, demonstrating that these two wind signals operate through completely different mechanisms at completely different timescales.

https://doi.org/10.5194/egusphere-2026-3546
Preprint. Discussion started: 7 August 2026
© Author(s) 2026. CC BY 4.0 License.

Among all drivers examined, ocean biological productivity showed the most consistent positive relationship with CCN in the 30-50° S latitude band, coinciding with the subtropical and subantarctic fronts, where trajectory-integrated chl a exposure at 24 to 48 hours was significantly correlated with CCN across all supersaturation levels. Outside this latitudinal band, the biological signal was weaker or not statistically significant. The polar band consistently showed the highest mean and median CCN concentrations across all five supersaturation levels, suggesting a persistent aerosol source near the sea-ice edge that operates continuously rather than episodically. The lower power-law exponent k in the polar band further supports the presence of freshly formed particles characteristic of the high-latitude Southern Ocean boundary layer. These findings highlight the need for direct in situ measurements of CCN sources, paired with collocated CCN observations, to quantify the biogenic aerosol pathway in the Indian Sector. Aerosol chemical composition measurements would further allow explicit identification of the sulfate, methanesulfonate, and organic contributions to CCN across supersaturation levels, directly addressing the uncertainty in aerosol source attribution that remains in this study. The dataset presented here establishes an essential observational baseline for the ISSO, provides a foundation for future process-level studies, and contributes to the sparse in situ aerosol record needed to evaluate and improve the representation of marine boundary layer CCN in climate models.

Data availability: All the observations have been uploaded to the Mendeley repository and can be accessed through: Mahajan, Anoop (2026), “Data for Exploring drivers of Cloud Condensation Nuclei in the Indian Sector of the Southern Ocean”, Mendeley Data, V1, doi: 10.17632/tydb7gwv53.1

Author contributions: SS and ASM conducted the CCN measurements during the expedition, performed data analysis, and wrote the manuscript. ASM served as the chief scientist during ISESO, overseeing all measurements, planning the study, and providing scientific supervision. SB and AS provided training on the CCN instrument, including its operation and data processing, before the expedition, as well as analysis of satellite-derived cloud droplet number concentrations. RK collected and provided black carbon and APS instrument data. SA and RKM provided in-situ chlorophyll a data. All authors contributed to the writing of the final manuscript.

https://doi.org/10.5194/egusphere-2026-3546
Preprint. Discussion started: 7 August 2026
© Author(s) 2026. CC BY 4.0 License.

Acknowledgements: The authors acknowledge the Ministry of Earth Sciences (MoES), Government of India, and the National Centre for Polar and Ocean Research (NCPOR) for organising and supporting the 12th Indian Scientific Expedition to the Southern Ocean (ISESO). We thank the captain and crew of the research vessel SA Agulhas for their support during the expedition. The contributions of all onboard scientists and technical staff involved in data collection are also gratefully acknowledged**.**

Financial support: This expedition was funded by the Ministry of Earth Sciences (MoES), Government of India, through the National Centre for Polar and Ocean Research (NCPOR), Goa, under the Indian Scientific Expeditions to the Southern Ocean programme (ISESO).

Competing interests. At least one of the co-authors is a member of the editorial board of Atmospheric Chemistry and Physics.

5 References

Andreae, M. O., Elbert, W., and De Mora, S. J.: Biogenic sulfur emissions and aerosols over the tropical South Atlantic. 3. Atmospheric dimethylsulfide, aerosols and cloud condensation nuclei, J. Geophys. Res., 100, 11335–11356, https://doi.org/10.1029/94jd02828, 1995.

Atkinson, H. M., Huang, R.-J., Chance, R., Roscoe, H. K., Hughes, C., Davison, B., Schönhardt, A., Mahajan, A. S., Saiz-Lopez, A., Hoffmann, T., and Liss, P. S.: Iodine emissions from the sea ice of the Weddell Sea, Atmos. Chem. Phys., 12, 11229–11244, https://doi.org/10.5194/acp-12-11229-2012, 2012.

Ayers, G. P. and Cainey, J. M.: The CLAW hypothesis: a review of the major developments, Environ. Chem., 4, 366–374, https://doi.org/10.1071/EN07080, 2007.

Ayers, G. P. and Gillett, R. W.: DMS and its oxidation products in the remote marine atmosphere: implications for climate and atmospheric chemistry, J. Sea Res., 43, 275–286, https://doi.org/10.1016/S1385-1101(00)00022-8, 2000.

https://doi.org/10.5194/egusphere-2026-3546
Preprint. Discussion started: 7 August 2026
© Author(s) 2026. CC BY 4.0 License.

Ayers, G. P. and Gras, J. L.: Seasonal relationship between cloud condensation nuclei and aerosol methanesulphonate in marine air, Nature., 353, 834–835, https://doi.org/10.1038/353834a0, 1991.

Baccarini, A., Dommen, J., Lehtipalo, K., Henning, S., Modini, R. L., Gysel-Beer, M., Baltensperger, U., and Schmale, J.: Low-Volatility Vapors and New Particle Formation Over the Southern Ocean During the Antarctic Circumnavigation Expedition, J. Geophys. Res. Atmos., 126, https://doi.org/10.1029/2021JD035126, 2021.

Bodas-Salcedo, A., Williams, K. D., Ringer, M. A., Beau, I., Cole, J. N. S., Dufresne, J.-L., Koshiro, T., Stevens, B., Wang, Z., and Yokohata, T.: Origins of the solar radiation biases over the Southern Ocean in CFMIP2 models, J. Clim., 27, 41–56, https://doi.org/10.1175/JCLI-D-13-00169.1, 2014.

Bougiatioti, A., Nenes, A., Fountoukis, C., Kalivitis, N., Pandis, S. N., and Mihalopoulos, N.: Size-resolved CCN distributions and activation kinetics of aged continental and marine aerosol, Atmos. Chem. Phys., 11, 8791–8808, https://doi.org/10.5194/acp-11-8791-2011, 2011.

de Bruyn, W. J., Harvey, M., Cainey, J. M., and Saltzman, E. S.: DMS and SO2 at Baring Head, New Zealand: Implications for the yield of SO2 from DMS, J. Atmos. Chem., 41, 189–209, https://doi.org/10.1023/A:1014252106572, 2002.

Carslaw, K. S., Lee, L. A., Reddington, C. L., Pringle, K. J., Rap, A., Forster, P. M., Mann, G. W., Spracklen, D. V., Woodhouse, M. T., Regayre, L. A., and Pierce, J. R.: Large contribution of natural aerosols to uncertainty in indirect forcing, Nature, 503, 67–71, https://doi.org/10.1038/nature12674, 2013.

Charlson, R. J., Lovelock, J. E., Andreae, M. O., and Warren, S. G.: Oceanic phytoplankton, atmospheric sulphur, cloud albedo and climate, Nature, 326, 655–661, https://doi.org/10.1038/326655a0, 1987.

Che, H., Stier, P., Watson-Parris, D., Gordon, H., and Deaconu, L.: Source attribution of cloud condensation nuclei and their impact on stratocumulus clouds and radiation in the south-eastern Atlantic, Atmos. Chem. Phys., 22, 10789–10807, https://doi.org/10.5194/acp-22-10789-2022, 2022.

https://doi.org/10.5194/egusphere-2026-3546
Preprint. Discussion started: 7 August 2026
© Author(s) 2026. CC BY 4.0 License.

694 Choudhury, G., Block, K., Haghighatnasab, M., Quaas, J., Goren, T., and Tesche, M.: Pristine
695 oceans are a significant source of uncertainty in quantifying global cloud condensation nuclei,
696 Atmos. Chem. Phys., 25, 3841–3856, https://doi.org/10.5194/acp-25-3841-2025, 2025.

697 Copernicus Marine Service: Global Ocean Colour (Copernicus-GlobColour), Bio-Geo-
698 Chemical, L4 (monthly and interpolated) from Satellite Observations (1997–ongoing),
699 Copernicus Marine Service, https://doi.org/10.48670/moi-00281, last access: 22 April 2025,
700 2023.

701 Downey, A., Jasper, J. D., Gras, J. J., and Whittlestone, S.: Lower tropospheric transport over
702 the Southern Ocean, J. Atmos. Chem., 11, 43–68, https://doi.org/10.1007/BF00053667, 1990.

703 Draxler, R., Stunder, B., Rolph, G., Stein, A., Taylor, A., Zinn, S., Loughner, C., and Crawford,
704 A.: HYSPLIT User's Guide, 2059–2077,
705 https://www.arl.noaa.gov/documents/reports/hysplit_user_guide.pdf, last access: 10 July 2025,
706 1999.

707 Drinovec, L., Močnik, G., Zotter, P., Prévôt, A. S. H., Ruckstuhl, C., Coz, E., Rupakheti, M.,
708 Sciare, J., Müller, T., Wiedensohler, A., and Hansen, A. D. A.: The "dual-spot" Aethalometer:
709 An improved measurement of aerosol black carbon with real-time loading compensation,
710 Atmos. Meas. Tech., 8, 1965–1979, https://doi.org/10.5194/amt-8-1965-2015, 2015.

711 Droplet Measurement Technologies: Cloud Condensation Nuclei (CCN) Counter Operator
712 Manual for Single-Column CCN, https://www.dropletmeasurement.com/manual/operations-
713 manual-cloud-condensation-nuclei-ccn-counter/, last access: 10 January 2025, 2017.

714 Dusek, U., Frank, G. P., Hildebrandt, L., Curtius, J., Schneider, J., Walter, S., Chand, D.,
715 Drewnick, F., Hings, S., Jung, D., Borrmann, S., and Andreae, M. O.: Size matters more than
716 chemistry for cloud-nucleating ability of aerosol particles, Science, 312, 1375–1378,
717 https://doi.org/10.1126/science.1125261, 2006.

718 Efraim, A., Rosenfeld, D., Schmale, J., and Zhu, Y.: Satellite retrieval of cloud condensation
719 nuclei concentrations in marine stratocumulus by using clouds as CCN chambers, J. Geophys.
720 Res. Atmos., 125, e2020JD032409, https://doi.org/10.1029/2020JD032409, 2020.

721 Fossum, K. N., Ovadnevaite, J., Ceburnis, D., Dall'Osto, M., Marullo, S., Bellacicco, M., Simó,
722 R., Liu, D., Flynn, M., Zuend, A., and O'Dowd, C.: Summertime Primary and Secondary

https://doi.org/10.5194/egusphere-2026-3546
Preprint. Discussion started: 7 August 2026
© Author(s) 2026. CC BY 4.0 License.

Contributions to Southern Ocean Cloud Condensation Nuclei, Sci. Rep., 8, 1–14, https://doi.org/10.1038/s41598-018-32047-4, 2018.

Gras, J. L.: Cloud condensation nuclei over the Southern Ocean, Geophys. Res. Lett., 17, 1565–1567, https://doi.org/10.1029/GL017i010p01565, 1990.

Grosvenor, D. P., Sourdeval, O., Zuidema, P., Ackerman, A., Alexandrov, M. D., Bennartz, R., Boers, R., Cairns, B., Chiu, J. C., Christensen, M., Deneke, H., Diamond, M., Feingold, G., Fridlind, A., Hünerbein, A., Knist, C., Kollias, P., Marshak, A., McCoy, D., Merk, D., Painemal, D., Rausch, J., Rosenfeld, D., Russchenberg, H., Seifert, P., Sinclair, K., Stier, P., van Diedenhoven, B., Wendisch, M., Werner, F., Wood, R., Zhang, Z., and Quaas, J.: Remote Sensing of Droplet Number Concentration in Warm Clouds: A Review of the Current State of Knowledge and Perspectives, Rev. Geophys., 56, 409–453, https://doi.org/10.1029/2017RG000593, 2018.

Gryspeerdt, E., McCoy, D. T., Crosbie, E., Moore, R. H., Nott, G. J., Painemal, D., Small-Griswold, J., Sorooshian, A., and Ziemba, L.: The impact of sampling strategy on the cloud droplet number concentration estimated from satellite data, Atmos. Meas. Tech., 15, 3875–3892, https://doi.org/10.5194/amt-15-3875-2022, 2022.

Halfter, S., Brokensha, L., Cotté, C., Eriksen, R., Friscourt, N., Green, D. B., Heil, P., Hellessey, N., Borreguero, L. H., Hirawake, T., Hobbs, W., Jansen, J., Mahajan, A. S., Makhado, A. B., McMahon, C. R., von der Meden, C. E. O., Raes, E., Stirnimann, L., Subramaniam, R., Sundaram, S., Tagliabue, A., Wynn-Edwards, C., Verhaegen, G., Tripathy, S. C., and Shadwick, E. H.: Status of ocean observations in the Indian Sector of the Southern Ocean, Elem Sci Anth, 13, https://doi.org/10.1525/elementa.2024.00098, 2025.

Hegg, D. A., Ferek, R. J., Hobbs, P. V., and Radke, L. F.: Dimethyl sulfide and cloud condensation nucleus correlations in the northeast Pacific Ocean, J. Geophys. Res., 96, https://doi.org/10.1029/91jd01309, 1991.

Heukelem, L. Van and Thomas, C. S.: Computer-assisted high-performance liquid chromatography method development with applications to the isolation and analysis of phytoplankton pigments, J. Chromatogr. A, 31–49, https://doi.org/10.1016/S0378-4347(00)00603-4, 2001.

https://doi.org/10.5194/egusphere-2026-3546
Preprint. Discussion started: 7 August 2026
© Author(s) 2026. CC BY 4.0 License.

Hudson, J. G. and Yum, S. S.: Cloud condensation nuclei spectra and polluted and clean clouds over the Indian Ocean, J. Geophys. Res. Atmos., 107, https://doi.org/10.1029/2001JD000829, 2002.

Hudson, J. G., Xie, Y., and Yum, S. S.: Vertical distributions of cloud condensation nuclei spectra over the summertime Southern Ocean, J. Geophys. Res. Atmos., 103, 16609–16624, https://doi.org/10.1029/97JD03438, 1998.

Hulswar, S., Simó, R., Galí, M., Bell, T. G., Lana, A., Inamdar, S., Halloran, P. R., Manville, G., and Mahajan, A. S.: Third revision of the global surface seawater dimethyl sulfide climatology (DMS-Rev3), Earth Syst. Sci. Data, 14, 2963–2987, https://doi.org/10.5194/essd-14-2963-2022, 2022.

Humphries, R. S., Keywood, M. D., Gribben, S., McRobert, I. M., Ward, J. P., Selleck, P., Taylor, S., Harnwell, J., Flynn, C., Kulkarni, G. R., Mace, G. G., Protat, A., Alexander, S. P., and McFarquhar, G.: Southern Ocean latitudinal gradients of cloud condensation nuclei, Atmos. Chem. Phys., 21, 12757–12782, https://doi.org/10.5194/acp-21-12757-2021, 2021.

Humphries, R. S., Keywood, M. D., Ward, J. P., Harnwell, J., Alexander, S. P., Klekociuk, A. R., Hara, K., Mcrobert, I. M., Protat, A., Alroe, J., Cravigan, L. T., Miljevic, B., Ristovski, Z. D., Schofield, R., Wilson, S. R., Flynn, C. J., Kulkarni, G. R., Mace, G. G., Mcfarquhar, G. M., Chambers, S. D., Williams, A. G., and Griffiths, A. D.: Measurement report: Understanding the seasonal cycle of Southern Ocean aerosols, Atmos. Chem. Phys., 23, 3749–3777, https://doi.org/10.5194/acp-23-3749-2023, 2023.

Hyder, P., Edwards, J. M., Allan, R. P., Hewitt, H. T., Bracegirdle, T. J., Gregory, J. M., Wood, R. A., Meijers, A. J. S., Mulcahy, J., Field, P., Furtado, K., Bodas-Salcedo, A., Williams, K. D., Copsey, D., Josey, S. A., Liu, C., Roberts, C. D., Sanchez, C., Ridley, J., Thorpe, L., Hardiman, S. C., Mayer, M., Berry, D. I., and Belcher, S. E.: Critical Southern Ocean climate model biases traced to atmospheric model cloud errors, Nat. Commun., 9, https://doi.org/10.1038/s41467-018-05634-2, 2018.

Inamdar, S., Tinel, L., Chance, R., Carpenter, L. J., Sabu, P., Chacko, R., Tripathy, S. C., Kerkar, A. U., Sinha, A. K., Bhaskar, P. V., Sarkar, A., Roy, R., Sherwen, T. T., Cuevas, C., Saiz-Lopez, A., Ram, K., and Mahajan, A. S.: Estimation of Reactive Inorganic Iodine Fluxes in the Indian and Southern Ocean Marine Boundary Layer, Atmos. Chem. Phys., 20, 12093–12114, https://doi.org/10.5194/acp-20-12093-2020, 2020.

https://doi.org/10.5194/egusphere-2026-3546
Preprint. Discussion started: 7 August 2026
© Author(s) 2026. CC BY 4.0 License.

(IPCC), I. P. on C. C. (Ed.): The Earth's Energy Budget, Climate Feedbacks and Climate Sensitivity, in: Climate Change 2021 – The Physical Science Basis: Working Group I Contribution to the Sixth Assessment Report of the Intergovernmental Panel on Climate Change, Cambridge University Press, Cambridge, 923–1054, https://doi.org/10.1017/9781009157896.009, 2023.

Joge, S. D., Mahajan, A. S., Hulswar, S., Marandino, C. A., Galí, M., Bell, T. G., and Simó, R.: Dimethyl sulfide (DMS) climatologies, fluxes, and trends – Part 1: Differences between seawater DMS estimations, Biogeosciences, 21, 4439–4452, https://doi.org/10.5194/bg-21-4439-2024, 2024.

Jokinen, T., Sipilä, M., Kontkanen, J., Vakkari, V., Tisler, P., Duplissy, E.-M., Junninen, H., Kangasluoma, J., Manninen, H. E., Petäjä, T., Kulmala, M., Worsnop, D. R., Kirkby, J., Virkkula, A., and Kerminen, V.-M.: Ion-induced sulfuric acid-ammonia nucleation drives particle formation in coastal Antarctica, Sci. Adv., https://doi.org/10.1126/sciadv.aat9744, 2018.

Kang, L., Marchand, R. T., Wood, R., and McCoy, I. L.: Coalescence Scavenging Drives Droplet Number Concentration in Southern Ocean Low Clouds, Geophys. Res. Lett., 49, https://doi.org/10.1029/2022GL097819, 2022.

Kilgour, D. B., Jernigan, C. M., Garmash, O., Aggarwal, S., Zhou, S., Mohr, C., Salter, M. E., Thornton, J. A., Wang, J., Zieger, P., and Bertram, T. H.: Cloud processing of dimethyl sulfide (DMS) oxidation products limits sulfur dioxide (SO2) and carbonyl sulfide (OCS) production in the eastern North Atlantic marine boundary layer, Atmos. Chem. Phys., 25, 1931–1947, https://doi.org/10.5194/acp-25-1931-2025, 2025.

Köhler, H.: The nucleus in and the growth of hygroscopic droplets, Trans. Faraday Soc., 32, 1152–1161, https://doi.org/10.1039/TF9363201152, 1936.

Korhonen, H., Carslaw, K. S., Spracklen, D. V., Mann, G. W., and Woodhouse, M. T.: Influence of oceanic dimethyl sulfide emissions on cloud condensation nuclei concentrations and seasonality over the remote Southern Hemisphere oceans: A global model study, J. Geophys. Res. Atmos., 113, 1–16, https://doi.org/10.1029/2007JD009718, 2008.

Lana, A., Simó, R., Vallina, S. M., and Dachs, J.: Potential for a biogenic influence on cloud microphysics over the ocean: A correlation study with satellite-derived data, Atmos. Chem. Phys., 12, 7977–7993, https://doi.org/10.5194/acp-12-7977-2012, 2012.

https://doi.org/10.5194/egusphere-2026-3546
Preprint. Discussion started: 7 August 2026
© Author(s) 2026. CC BY 4.0 License.

Lizotte, M. P.: The Contributions of Sea Ice Algae to Antarctic Marine Primary Production, Am. Zool., 41, 57–73, https://doi.org/10.1093/icb/41.1.57, 2001.

Mace, G. G., Protat, A., Humphries, R. S., Alexander, S. P., McRobert, I. M., Ward, J., Selleck, P., Keywood, M., and McFarquhar, G. M.: Southern Ocean Cloud Properties Derived From CAPRICORN and MARCUS Data, J. Geophys. Res. Atmos., 126, https://doi.org/10.1029/2020JD033368, 2021.

Mace, G. G., Benson, S., Humphries, R., Gombert, P. M., and Sterner, E.: Natural marine cloud brightening in the Southern Ocean, Atmos. Chem. Phys., 23, 1677–1685, https://doi.org/10.5194/acp-23-1677-2023, 2023.

Mahajan, A. S., Fadnavis, S., Thomas, M. A., Pozzoli, L., Gupta, S., Royer, S., Saiz-Lopez, A., and Simó, R.: Quantifying the impacts of an updated global dimethyl sulfide climatology on cloud microphysics and aerosol radiative forcing, J. Geophys. Res. Atmos., 120, 1–13, https://doi.org/10.1002/2014JD022687, 2015.

Mahajan, A. S., Biswas, M. S., Beirle, S., Wagner, T., Schönhardt, A., Benavent, N., and Saiz-Lopez, A.: Observations of iodine monoxide over three summers at the Indian Antarctic bases of Bharati and Maitri, Atmos. Chem. Phys., 21, 11829–11842, https://doi.org/10.5194/acp-21-11829-2021, 2021.

Mahilang, M., Deb, M. K., Pervez, S., Tiwari, S., and Jain, V. K.: Biogenic secondary organic aerosol formation in an urban area of eastern central India: Seasonal variation, size distribution and source characterization, Environ. Res., 195, 110802, https://doi.org/10.1016/j.envres.2021.110802, 2021.

Mallet, M. D., Humphries, R. S., Fiddes, S. L., Alexander, S. P., Altieri, K., Angot, H., Anilkumar, N., Bartels-Rausch, T., Creamean, J., Dall'Osto, M., Dommergue, A., Frey, M., Henning, S., Lannuzel, D., Lapere, R., Mace, G. G., Mahajan, A. S., McFarquhar, G. M., Meiners, K. M., Miljevic, B., Peeken, I., Protat, A., Schmale, J., Steiner, N., Sellegri, K., Simó, R., Thomas, J. L., Willis, M. D., Winton, V. H. L., and Woodhouse, M. T.: Untangling the influence of Antarctic and Southern Ocean life on clouds, Elem. Sci. Anth., 11, https://doi.org/10.1525/elementa.2022.00130, 2023.

Mansour, K., Decesari, S., Ceburnis, D., Ovadnevaite, J., and Rinaldi, M.: Machine learning for prediction of daily sea surface dimethylsulfide concentration and emission flux over the

https://doi.org/10.5194/egusphere-2026-3546
Preprint. Discussion started: 7 August 2026
© Author(s) 2026. CC BY 4.0 License.

North Atlantic Ocean (1998–2021), Sci. Total Environ., 871, https://doi.org/10.1016/j.scitotenv.2023.162123, 2023.

Manville, G., Bell, T. G., Mulcahy, J. P., Simó, R., Galí, M., Mahajan, A. S., Hulswar, S., and Halloran, P. R.: Global analysis of the controls on seawater dimethylsulfide spatial variability, Biogeosciences, 20, 1813–1828, https://doi.org/10.5194/bg-20-1813-2023, 2023.

McCoy, D. T., Burrows, S. M., Wood, R., Grosvenor, D. P., Elliott, S. M., Ma, P. L., Rasch, P. J., and Hartmann, D. L.: Natural aerosols explain seasonal and spatial patterns of Southern Ocean cloud albedo, Sci. Adv., 1, https://doi.org/10.1126/sciadv.1500157, 2015.

McCoy, I. L., McCoy, D. T., Wood, R., Regayre, L., Watson-Parris, D., Grosvenor, D. P., Mulcahy, J. P., Hu, Y., Bender, F. A. M., Field, P. R., Carslaw, K. S., and Gordon, H.: The hemispheric contrast in cloud microphysical properties constrains aerosol forcing, Proc. Natl. Acad. Sci. U. S. A., 117, 18998–19006, https://doi.org/10.1073/pnas.1922502117, 2020.

McCoy, I. L., Bretherton, C. S., Wood, R., Twohy, C. H., Gettelman, A., Bardeen, C. G., and Toohey, D. W.: Influences of Recent Particle Formation on Southern Ocean Aerosol Variability and Low Cloud Properties, J. Geophys. Res. Atmos., 126, 1–27, https://doi.org/10.1029/2020JD033529, 2021.

McFarquhar, G., Marchand, R., Bretherton, C., Alexander, S., Protat, A., Siems, S., Wood, R., and DeMott, P.: Measurements of Aerosols, Radiation, and Clouds over the Southern Ocean (MARCUS) Field Campaign Report, DOE/SC-ARM-19-008, U.S. Department of Energy, Office of Science, Atmospheric Radiation Measurement (ARM) User Facility, https://www.osti.gov/biblio/1524775, 2019.

McFarquhar, G. M., Bretherton, C. S., Marchand, R., Protat, A., DeMott, P. J., Alexander, S. P., Roberts, G. C., Twohy, C. H., Toohey, D., Siems, S., Huang, Y., Wood, R., Rauber, R. M., Lasher-Trapp, S., Jensen, J., Stith, J. L., Mace, J., Um, J., Järvinen, E., Schnaiter, M., Gettelman, A., Sanchez, K. J., McCluskey, C. S., Russell, L. M., McCoy, I. L., Atlas, R. L., Bardeen, C. G., Moore, K. A., Hill, T. C. J., Humphries, R. S., Keywood, M. D., Ristovski, Z., Cravigan, L., Schofield, R., Fairall, C., Mallet, M. D., Kreidenweis, S. M., Rainwater, B., D'Alessandro, J., Wang, Y., Wu, W., Saliba, G., Levin, E. J. T., Ding, S., Lang, F., Truong, S. C. H., Wolff, C., Haggerty, J., Harvey, M. J., Klekociuk, A. R., and McDonald, A.: Observations of clouds, aerosols, precipitation, and surface radiation over the southern ocean, Bull. Am. Meteorol. Soc., 102, E894–E928, https://doi.org/10.1175/BAMS-D-20-0132.1, 2021.

https://doi.org/10.5194/egusphere-2026-3546
Preprint. Discussion started: 7 August 2026
© Author(s) 2026. CC BY 4.0 License.

Muhlbauer, A., Hashino, T., Xue, L., Teller, A., Lohmann, U., Rasmussen, R. M., Geresdi, I., and Pan, Z.: Intercomparison of aerosol-cloud-precipitation interactions in stratiform orographic mixed-phase clouds, Atmos. Chem. Phys., 10, 8173–8196, https://doi.org/10.5194/acp-10-8173-2010, 2010.

Niu, Q., McFarquhar, G. M., Marchand, R., Theisen, A., Cavallo, S. M., Flynn, C., DeMott, P. J., McCluskey, C. S., Humphries, R. S., and Hill, T. C. J.: 62° S Witnesses the Transition of Boundary Layer Marine Aerosol Pattern Over the Southern Ocean (50° S–68° S, 63° E–150° E) During the Spring and Summer: Results From MARCUS (I), J. Geophys. Res. Atmos., 129, https://doi.org/10.1029/2023JD040396, 2024.

Novak, G. A., Fite, C. H., Holmes, C. D., Veres, P. R., Neuman, J. A., Faloona, I., Thornton, J. A., Wolfe, G. M., Vermeuel, M. P., Jernigan, C. M., Peischl, J., Ryerson, T. B., Thompson, C. R., Bourgeois, I., Warneke, C., Gkatzelis, G. I., Coggon, M. M., Sekimoto, K., Bui, T. P., Dean-Day, J., Diskin, G. S., DiGangi, J. P., Nowak, J. B., Moore, R. H., Wiggins, E. B., Winstead, E. L., Robinson, C., Thornhill, K. L., Sanchez, K. J., Hall, S. R., Ullmann, K., Dollner, M., Weinzierl, B., Blake, D. R., and Bertram, T. H.: Rapid cloud removal of dimethyl sulfide oxidation products limits SO2 and cloud condensation nuclei production in the marine atmosphere, Proc. Natl. Acad. Sci. U. S. A., 118, https://doi.org/10.1073/pnas.2110472118, 2021.

Paramonov, M., Kerminen, V. M., Gysel, M., Aalto, P. P., Andreae, M. O., Asmi, E., Baltensperger, U., Bougiatioti, A., Brus, D., Frank, G. P., Good, N., Gunthe, S. S., Hao, L., Irwin, M., Jaatinen, A., Jurányi, Z., King, S. M., Kortelainen, A., Kristensson, A., Lihavainen, H., Kulmala, M., Lohmann, U., Martin, S. T., McFiggans, G., Mihalopoulos, N., Nenes, A., O'Dowd, C. D., Ovadnevaite, J., Petäjä, T., Pöschl, U., Roberts, G. C., Rose, D., Svenningsson, B., Swietlicki, E., Weingartner, E., Whitehead, J., Wiedensohler, A., Wittbom, C., and Sierau, B.: A synthesis of cloud condensation nuclei counter (CCNC) measurements within the EUCAARI network, Atmos. Chem. Phys., 15, 12211–12229, https://doi.org/10.5194/acp-15-12211-2015, 2015.

Pfeifer, S., Müller, T., Weinhold, K., Zikova, N., Dos Santos, S. M., Marinoni, A., Bischof, O. F., Kykal, C., Ries, L., Meinhardt, F., Aalto, P., Mihalopoulos, N., and Wiedensohler, A.: Intercomparison of 15 aerodynamic particle size spectrometers (APS 3321): Uncertainties in particle sizing and number size distribution, Atmos. Meas. Tech., 9, 1545–1551, https://doi.org/10.5194/amt-9-1545-2016, 2016.

https://doi.org/10.5194/egusphere-2026-3546
Preprint. Discussion started: 7 August 2026
© Author(s) 2026. CC BY 4.0 License.

907 Pierce, J. R. and Adams, P. J.: Global evaluation of CCN formation by direct emission of sea
908 salt and growth of ultrafine sea salt, J. Geophys. Res. Atmos., 111, 1–16,
909 https://doi.org/10.1029/2005JD006186, 2006.

910 Pierce, J. R. and Adams, P. J.: Uncertainty in global CCN concentrations from uncertain aerosol
911 nucleation and primary emission rates, Atmos. Chem. Phys., 9, 1339–1356,
912 https://doi.org/10.5194/acp-9-1339-2009, 2009.

913 Price, R., Orr, A., Field, P. R., Mace, G., and Protat, A.: Simulation of Southern Ocean cloud
914 processes using the high-resolution regional UK Met Office Unified Model with interactive
915 aerosols, ESS Open Archive [preprint],
916 https://doi.org/10.22541/essoar.172280700.08183709/v1, 2024.

917 Quinn, P. K. and Bates, T. S.: The case against climate regulation via oceanic phytoplankton
918 sulphur emissions., Nature, 480, 51–56, https://doi.org/10.1038/nature10580, 2011.

919 Quinn, P. K., Bates, T. S., Miller, T. L., Coffman, D. J., Johnson, J. E., Harris, J. M., Ogren, J.
920 A., Forbes, G., Anderson, T. L., Covert, D. S., and Rood, M. J.: Surface submicron aerosol
921 chemical composition: What fraction is not sulfate?, J. Geophys. Res. Atmos., 105, 6785–6805,
922 https://doi.org/10.1029/1999JD901034, 2000.

923 Quinn, P. K., Coffman, D. J., Johnson, J. E., Upchurch, L. M., and Bates, T. S.: Small fraction
924 of marine cloud condensation nuclei made up of sea spray aerosol, Nat. Geosci., 10, 674–679,
925 https://doi.org/10.1038/ngeo3003, 2017.

926 Roberts, G. C. and Nenes, A.: A continuous-flow streamwise thermal-gradient CCN chamber
927 for atmospheric measurements, Aerosol Sci. Technol., 39, 206–221,
928 https://doi.org/10.1080/027868290913988, 2005.

929 Roscoe, H. K., Jones, A. E., Brough, N., Weller, R., Saiz-Lopez, A., Mahajan, A. S.,
930 Schönhardt, A., Burrows, J. P., and Fleming, Z. L.: Particles and iodine compounds in coastal
931 Antarctica, J. Geophys. Res. Atmos., 120, https://doi.org/10.1002/2015JD023301, 2015.

932 Rosenfeld, D., Andreae, M. O., Asmi, A., Chin, M., de Leeuw, G., Donovan, D. P., Kahn, R.,
933 Kinne, S., Kivekäs, N., Kulmala, M., Lau, W., Schmidt, K. S., Suni, T., Wagner, T., Wild, M.,
934 and Quaas, J.: Global observations of aerosol-cloud-precipitation-climate interactions, Rev.
935 Geophys., 52, 750–808, https://doi.org/10.1002/2013RG000441, 2014.

https://doi.org/10.5194/egusphere-2026-3546
Preprint. Discussion started: 7 August 2026
© Author(s) 2026. CC BY 4.0 License.

936 Twomey, S: The Influence of Pollution on the Shortwave Albedo of Clouds, J. Atmos. Sci., 34,
937 1149-1152, https://doi.org/10.1175/1520-0469(1977)034%3C1149:TIOPOT%3E2.0.CO;2,
938 1977.

939 Saiz-Lopez, A., Blaszczak-Boxe, C. S., and Carpenter, L. J.: A mechanism for biologically
940 induced iodine emissions from sea ice, Atmos. Chem. Phys., 15, 9731–9746,
941 https://doi.org/10.5194/acp-15-9731-2015, 2015.

942 Saliba, G., Sanchez, K. J., Russell, L. M., Twohy, C. H., Roberts, G. C., Lewis, S., Dedrick, J.,
943 McCluskey, C. S., Moore, K., DeMott, P. J., and Toohey, D. W.: Organic composition of three
944 different size ranges of aerosol particles over the Southern Ocean, Aerosol Sci. Technol., 55,
945 268–288, https://doi.org/10.1080/02786826.2020.1845296, 2020.

946 Salim, S. N., Adhikari, A., Menon, H. B., Kumar, N. V. P. K., and Kunjukrishnapillai, R.:
947 Thermodynamic characteristics of marine atmospheric boundary layer across frontal regions
948 of the Indian Ocean Sector of the Southern Ocean based on three field campaigns, Atmos. Res.,
949 286, 106678, https://doi.org/10.1016/j.atmosres.2023.106678, 2023.

950 Sanchez, K. J., Chen, C. L., Russell, L. M., Betha, R., Liu, J., Price, D. J., Massoli, P., Ziemba,
951 L. D., Crosbie, E. C., Moore, R. H., Müller, M., Schiller, S. A., Wisthaler, A., Lee, A. K. Y.,
952 Quinn, P. K., Bates, T. S., Porter, J., Bell, T. G., Saltzman, E. S., Vaillancourt, R. D., and
953 Behrenfeld, M. J.: Substantial Seasonal Contribution of Observed Biogenic Sulfate Particles to
954 Cloud Condensation Nuclei, Sci. Rep., 8, 1–14, https://doi.org/10.1038/s41598-018-21590-9,
955 2018.

956 Sanchez, K. J., Roberts, G. C., Saliba, G., Russell, L. M., Twohy, C., Reeves, J. M., Humphries,
957 R. S., Keywood, M. D., Ward, J. P., and McRobert, I. M.: Measurement report: Cloud processes
958 and the transport of biological emissions affect southern ocean particle and cloud condensation
959 nuclei concentrations, Atmos. Chem. Phys., 21, 3427–3446, https://doi.org/10.5194/acp-21-
960 3427-2021, 2021.

961 Schmale, J., Baccarini, A., Thurnherr, I., Henning, S., Efraim, A., Regayre, L., Bolas, C.,
962 Hartmann, M., Welti, A., Lehtipalo, K., Aemisegger, F., Tatzelt, C., Landwehr, S., Modini, R.
963 L., Tummon, F., Johnson, J. S., Harris, N., Schnaiter, M., Toffoli, A., Derkani, M., Bukowiecki,
964 N., Stratmann, F., Dommen, J., Sperger, U. B., Wernli, H., Rosenfeld, D., Gysel-Beer, M., and
965 Carslaw, K. S.: Overview of the antarctic circumnavigation expedition: Study of preindustrial-

https://doi.org/10.5194/egusphere-2026-3546
Preprint. Discussion started: 7 August 2026
© Author(s) 2026. CC BY 4.0 License.

like aerosols and their climate effects (ACE-SPACE), Bull. Am. Meteorol. Soc., 100, 2260–2283, https://doi.org/10.1175/BAMS-D-18-0187.1, 2019.

Shindell, D. T., Lamarque, J. F., Schulz, M., Flanner, M., Jiao, C., Chin, M., Young, P. J., Lee, Y. H., Rotstayn, L., Mahowald, N., Milly, G., Faluvegi, G., Balkanski, Y., Collins, W. J., Conley, A. J., Dalsoren, S., Easter, R., Ghan, S., Horowitz, L., Liu, X., Myhre, G., Nagashima, T., Naik, V., Rumbold, S. T., Skeie, R., Sudo, K., Szopa, S., Takemura, T., Voulgarakis, A., Yoon, J. H., and Lo, F.: Radiative forcing in the ACCMIP historical and future climate simulations, Atmos. Chem. Phys., 13, 2939–2974, https://doi.org/10.5194/acp-13-2939-2013, 2013.

Singh, M., Kondo, Y., Ohata, S., Mori, T., Oshima, N., Hyvärinen, A., Backman, J., Asmi, E., Servomaa, H., Schnaiter, F. M., Andrews, E., Sharma, S., Eleftheriadis, K., Vratolis, S., Zhao, Y., Koike, M., Moteki, N., and Sinha, P. R.: Mass absorption cross section of black carbon for Aethalometer in the Arctic, Aerosol Sci. Technol., 58, 536–553, https://doi.org/10.1080/02786826.2024.2316173, 2024.

Sipilä, M., Sarnela, N., Jokinen, T., Henschel, H., Junninen, H., Kontkanen, J., Richters, S., Kangasluoma, J., Franchin, A., Peräkylä, O., Rissanen, M. P., Ehn, M., Vehkamäki, H., Kurten, T., Berndt, T., Petäjä, T., Worsnop, D., Ceburnis, D., Kerminen, V. M., Kulmala, M., and O'Dowd, C.: Molecular-scale evidence of aerosol particle formation via sequential addition of HIO3, Nature, 537, 532–534, https://doi.org/10.1038/nature19314, 2016.

Smith, D. K. E., Renfrew, I. A., van den Heuvel, F., Lachlan-Cope, T., Crawford, I., Bower, K., Flynn, M., Evans, M. D., Abel, S. J., and Field, P.: The Impact of Mixed-Phase Cloud Processes on Simulating Southern Ocean Clouds and Their Radiative Effect, J. Geophys. Res. Atmos., 130, https://doi.org/10.1029/2025JD044452, 2025.

Svensmark, H., Enghoff, M. B., Svensmark, J., Thaler, I., and Shaviv, N. J.: Supersaturation and Critical Size of Cloud Condensation Nuclei in Marine Stratus Clouds, Geophys. Res. Lett., 51, https://doi.org/10.1029/2024GL108140, 2024.

Tatzelt, C., Henning, S., Welti, A., Baccarini, A., Hartmann, M., Gysel-Beer, M., Van Pinxteren, M., Modini, R. L., Schmale, J., and Stratmann, F.: Circum-Antarctic abundance and properties of CCN and INPs, Atmos. Chem. Phys., 22, 9721–9745, https://doi.org/10.5194/acp-22-9721-2022, 2022.

https://doi.org/10.5194/egusphere-2026-3546
Preprint. Discussion started: 7 August 2026
© Author(s) 2026. CC BY 4.0 License.

Tulet, P., Van Baelen, J., Bosser, P., Brioude, J., Colomb, A., Goloub, P., Pazmino, A., Portafaix, T., Ramonet, M., Sellegri, K., Thyssen, M., Gest, L., Marquestaut, N., Mékiès, D., Metzger, J. M., Athier, G., Blarel, L., Delmotte, M., Desprairies, G., Dournaux, M., Dubois, G., Duflot, V., Lamy, K., Gardes, L., Guillemot, J. F., Gros, V., Kolasinski, J., Lopez, M., Magand, O., Noury, E., Nunes-Pinharanda, M., Payen, G., Pianezze, J., Picard, D., Picard, O., Prunier, S., Rigaud-Louise, F., Sicard, M., and Torres, B.: MAP-IO: an atmospheric and marine observatory program on board Marion Dufresne over the Southern Ocean, Earth Syst. Sci. Data, 16, 3821–3849, https://doi.org/10.5194/essd-16-3821-2024, 2024.

Twohy, C. H., DeMott, P. J., Russell, L. M., Toohey, D. W., Rainwater, B., Geiss, R., Sanchez, K. J., Lewis, S., Roberts, G. C., Humphries, R. S., McCluskey, C. S., Moore, K. A., Selleck, P. W., Keywood, M. D., Ward, J. P., and McRobert, I. M.: Cloud-Nucleating Particles Over the Southern Ocean in a Changing Climate, Earth's Future, 9, https://doi.org/10.1029/2020EF001673, 2021.

Twomey, S.: The nuclei of natural cloud formation part II: The supersaturation in natural clouds and the variation of cloud droplet concentration, Geofis. Pura Appl., 43, 243–249, https://doi.org/10.1007/BF01993560, 1959.

Uetake, J., Hill, T. C. J., Moore, K. A., DeMott, P. J., Protat, A., and Kreidenweis, S. M.: Airborne bacteria confirm the pristine nature of the Southern Ocean boundary layer, Proc. Natl. Acad. Sci. U. S. A., 117, 13275–13282, https://doi.org/10.1073/pnas.2000134117, 2020.

Vallina, S. M., Simó, R., and Gassó, S.: What controls CCN seasonality in the Southern Ocean? A statistical analysis based on satellite-derived chlorophyll and CCN and model-estimated OH radical and rainfall, Global Biogeochem. Cycles, 20, https://doi.org/10.1029/2005GB002597, 2006.

Wiedensohler, A., Birmili, W., Putaud, J., and Ogren, J.: Recommendations for Aerosol Sampling, in: Aerosol Science: Technology and Applications, 2nd Edn., edited by: Colbeck, I. and Lazaridis, M., Wiley, Chichester, 45–59, https://doi.org/10.1002/9781118682555.ch3, 2013.

Wohl, C., Villamayor, J., Galí, M., Mahajan, A. S., Fernández, R. P., Cuevas, C. A., Bossolasco, A., Li, Q., Kettle, A. J., Williams, T., Sarda-Esteve, R., Gros, V., Simó, R., and Saiz-Lopez, A.: Marine emissions of methanethiol increase aerosol cooling in the Southern Ocean, Sci. Adv., 10, 2465, https://doi.org/10.1126/sciadv.adq2465, 2024.

https://doi.org/10.5194/egusphere-2026-3546
Preprint. Discussion started: 7 August 2026
© Author(s) 2026. CC BY 4.0 License.

Wood, R., Leon, D., Lebsock, M., Snider, J., and Clarke, A. D.: Precipitation driving of droplet concentration variability in marine low clouds, J. Geophys. Res. Atmos., 117, https://doi.org/10.1029/2012JD018305, 2012.

Zheng, G., Kuang, C., Uin, J., Watson, T., and Wang, J.: Large contribution of organics to condensational growth and formation of cloud condensation nuclei (CCN) in the remote marine boundary layer, Atmos. Chem. Phys., 20, 12515–12525, https://doi.org/10.5194/acp-20-12515-2020, 2020.

Zheng, X., Dong, X., Xi, B., Logan, T., and Wang, Y.: Distinctive aerosol–cloud–precipitation interactions in marine boundary layer clouds from the ACE-ENA and SOCRATES aircraft field campaigns, Atmos. Chem. Phys., 24, 10323–10347, https://doi.org/10.5194/acp-24-10323-2024, 2024.

https://doi.org/10.5194/egusphere-2026-3546
Preprint. Discussion started: 7 August 2026
© Author(s) 2026. CC BY 4.0 License.

1039 Tables and Figures

1040 **Table 1**: Different datasets used in this study, including in situ observations, reanalysis data
1041 and satellite observations.

Dataset	Type	Source/Instrument	Resolution	Parameter	Unit
CCN	In-situ Observation	Cloud Condensation Nuclei Counter (DMT-100)	Along the ship track; 1 s	CCN number concentration	cm^{-3}
Wind Speed	Reanalysis	ERA5 (ECMWF)	Daily; 0.25°× 0.25°	10 m wind speed	$m\ s^{-1}$
Wind Speed	In-situ Observation	Automated Weather Station (AWS)	Along the ship track; 1 s	Wind Speed	$m\ s^{-1}$
Chlorophyll-a Exposure	Satellite Remote Sensing	Copernicus Glob Colour	Daily; 0.042°× 0.042°	Chlorophyll a concentration	$mg\ m^{-3}$
APS	In-situ Observation	Aerodynamical Particle Sizer	Along the ship track; 5 min	Total number concentration	cm^{-3}
HYSPLIT Trajectories	Lagrangian Model	NOAA HYSPLIT with ERA5 inputs	6-hourly; 0.25°× 0.25°	Air parcel trajectories, altitudes	-

1042

1043

1044 **Table 2**: Statistical summary of cloud condensation nuclei (CCN) concentrations (cm^{-3})
1045 measured at supersaturation levels (*S*) of 0.2%, 0.4%, 0.6%, 0.8%, and 1.0% across five
1046 latitude bands (20-30° S to 60-70° S) over the Indian Sector of the Southern Ocean.
1047 Statistics include the minimum, 10th percentile, 25th percentile, mean, standard deviation

https://doi.org/10.5194/egusphere-2026-3546
Preprint. Discussion started: 7 August 2026
© Author(s) 2026. CC BY 4.0 License.

(SD), median, 75th percentile, 90th percentile, maximum, and the number of data points (n), all in units of cm^{-3}, for each latitude band.

							Percentiles				
S (%)	Latitude (° S)	Mean	Median	SD	Min	Max	10th	25th	75th	90th	n
CCN 0.2	20-30	105	112	53	25	203	37	52	148	177	228
	30-40	124	134	48	39	228	56	80	164	183	541
	40-50	153	163	73	9	347	48	101	192	248	664
	50-60	129	126	63	11	331	46	77	176	215	574
	60-70	175	181	49	35	332	99	154	208	229	668
CCN 0.4	20-30	130	132	63	35	294	48	73	173	216	116
	30-40	156	155	56	57	276	81	107	204	229	297
	40-50	178	184	84	13	382	57	115	236	285	388
	50-60	165	154	85	16	485	68	103	206	289	305
	60-70	239	255	59	80	397	144	205	279	301	323
CCN 0.6	20-30	183	188	78	42	342	72	120	240	295	138
	30-40	204	206	70	52	373	119	144	252	294	390
	40-50	216	222	94	15	481	82	150	279	334	456
	50-60	216	191	108	20	486	82	142	287	378	438
	60-70	283	286	72	96	456	184	234	329	370	404
CCN 0.8	20-30	216	221	93	47	470	88	139	276	331	115
	30-40	243	242	78	102	445	149	179	292	344	337
	40-50	244	253	104	14	470	86	167	319	380	413
	50-60	246	227	113	26	499	108	169	330	413	302
	60-70	310	311	72	137	499	214	263	359	390	306
CCN 1.0	20-30	276	294	89	85	444	128	234	340	381	80
	30-40	289	297	82	120	497	179	223	341	385	287
	40-50	275	286	115	12	498	104	200	357	424	423
	50-60	253	237	118	32	500	99	168	342	433	381
	60-70	326	323	74	125	499	230	274	380	421	292

https://doi.org/10.5194/egusphere-2026-3546
Preprint. Discussion started: 7 August 2026
© Author(s) 2026. CC BY 4.0 License.

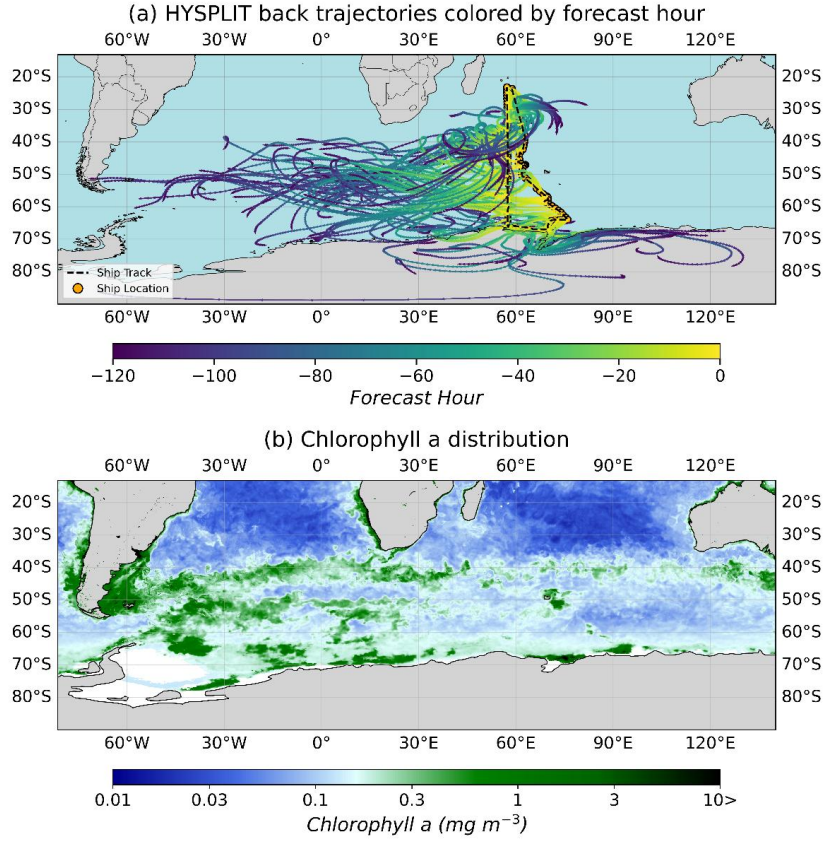

Figure 1: (a) Five-day HYSPLIT back trajectories computed at 6-hour intervals for air masses arriving along the cruise track of the 12th Indian Scientific Expedition to the Southern Ocean (ISESO-12). Trajectories are coloured by forecast hour, and the cruise track and sampling location are indicated. (b) Chlorophyll a distribution over the Southern Ocean is used to characterise the biological productivity encountered by the air masses.

https://doi.org/10.5194/egusphere-2026-3546
Preprint. Discussion started: 7 August 2026
© Author(s) 2026. CC BY 4.0 License.

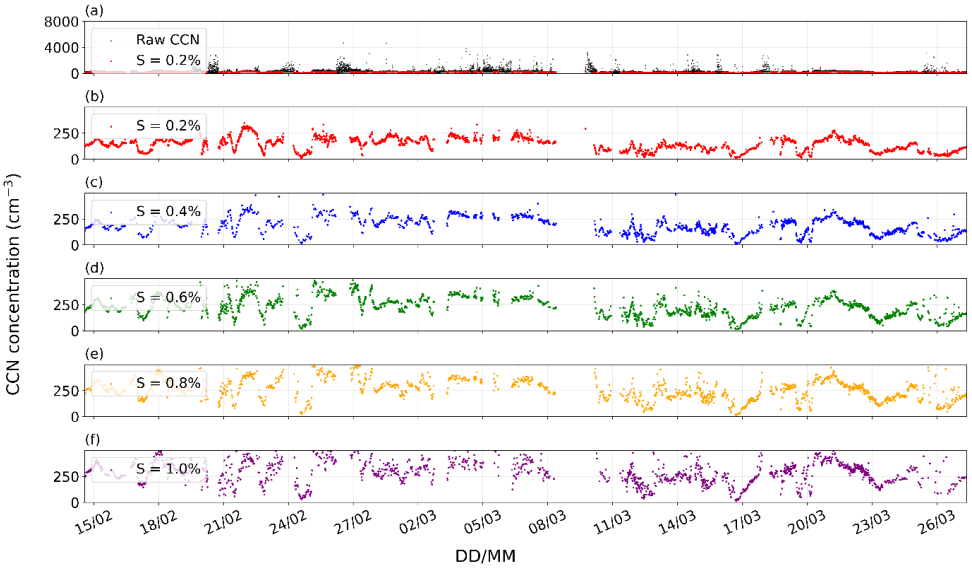

1072

1073 **Figure 2:** Time series of raw CCN observations (black) and filtered CCN concentrations
1074 at S = 0.2% (red) during the expedition. The lower panels show the filtered CCN
1075 concentrations at individual supersaturation levels (S = 0.2%, 0.4%, 0.6%, 0.8%, and
1076 1.0%).

1077

https://doi.org/10.5194/egusphere-2026-3546
Preprint. Discussion started: 7 August 2026
© Author(s) 2026. CC BY 4.0 License.

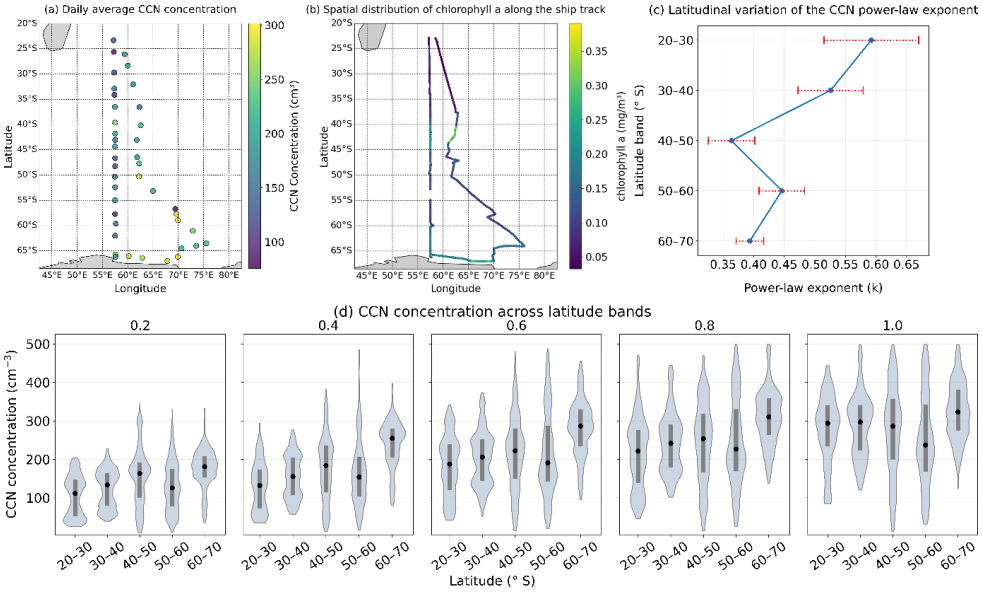

Figure 3. Spatial and latitudinal variability of CCN concentrations, chlorophyll a, and the CCN power-law exponent during the 12th Indian Scientific Expedition to the Southern Ocean (ISESO-12). (a) Daily average CCN concentration along the ship track. (b) Spatial distribution of chlorophyll a along the ship track. (c) Latitudinal variation of the CCN power-law exponent (k), which characterises the dependence of CCN concentration on supersaturation. (d) Distribution of CCN concentrations at five supersaturation levels (S = 0.2%, 0.4%, 0.6%, 0.8%, and 1.0%) across latitude bands (20–30°S to 60–70°S), illustrating the latitudinal variability in CCN concentration.

https://doi.org/10.5194/egusphere-2026-3546
Preprint. Discussion started: 7 August 2026
© Author(s) 2026. CC BY 4.0 License.

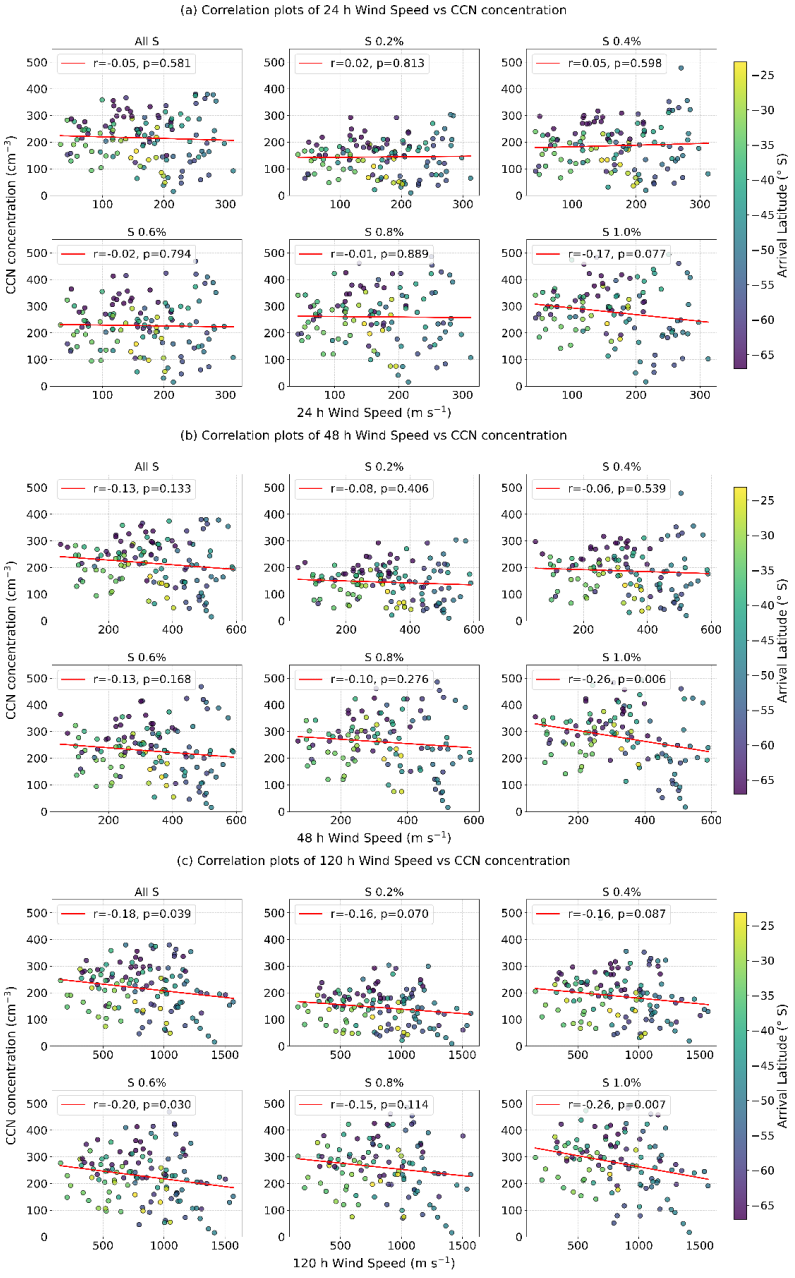

Figure 4: Correlation between CCN concentration and wind speed along back trajectories for (a) 24 h, (b) 48 h, and (c) 120 h exposure periods. Each panel presents results for all supersaturation levels combined and for individual supersaturation levels (S = 0.2%, 0.4%, 0.6%, 0.8%, and 1.0%). Scatter points are coloured by arrival latitude, and the red line represents the linear regression fit. The consistently weak or negative correlations

https://doi.org/10.5194/egusphere-2026-3546
Preprint. Discussion started: 7 August 2026
© Author(s) 2026. CC BY 4.0 License.

1093 across all supersaturation levels and exposure periods indicate that integrated wind speed
1094 has limited influence on CCN concentrations.

https://doi.org/10.5194/egusphere-2026-3546
Preprint. Discussion started: 7 August 2026
© Author(s) 2026. CC BY 4.0 License.

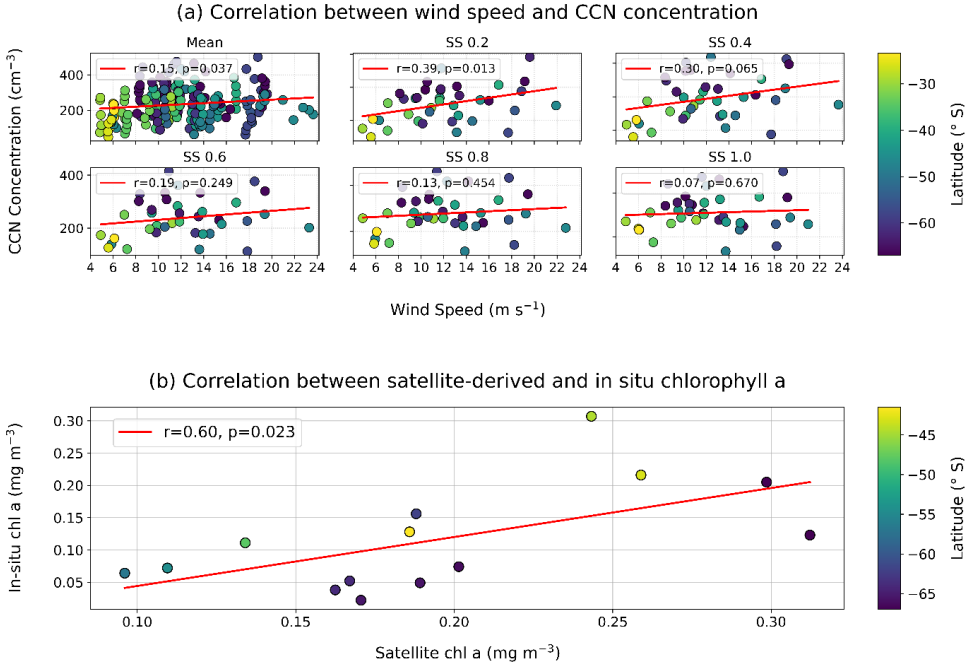

Figure 5: (a) Correlation of daily mean in-situ wind speed vs CCN concentration at all S levels. Significant positive correlations were seen at $S = 0.2\%$ ($r = 0.39$, $p = 0.01$) and in the overall mean ($r = 0.15$, $p = 0.04$), reflecting local sea-spray production. (b) Correlation between daily mean satellite-derived chlorophyll a and in situ measured chlorophyll a concentration along the ship track. Points are coloured by latitude. The red line shows the linear regression fit.

https://doi.org/10.5194/egusphere-2026-3546
Preprint. Discussion started: 7 August 2026
© Author(s) 2026. CC BY 4.0 License.

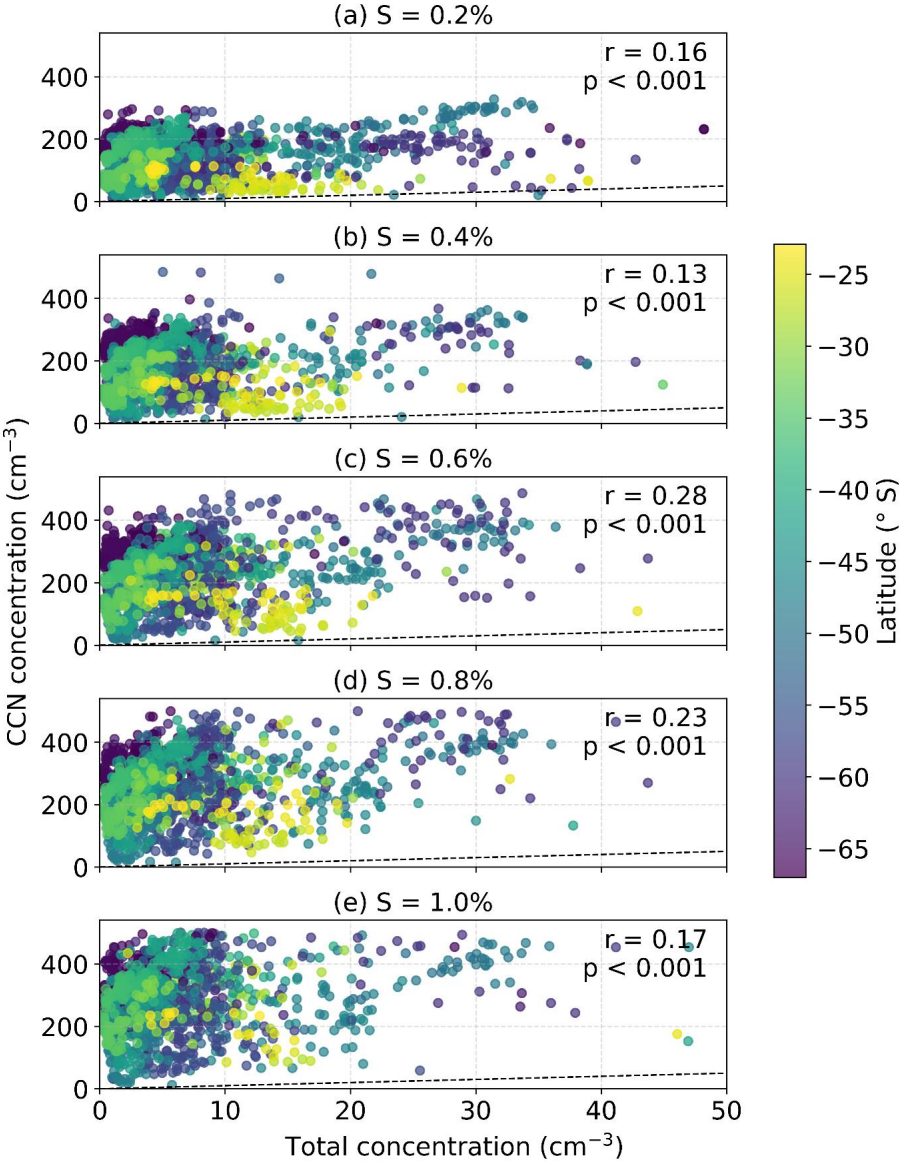

Figure 6: Scatter plots showing the relationship between APS total particle concentration and CCN concentration at supersaturation levels of (a) 0.2%, (b) 0.4%, (c) 0.6%, (d) 0.8%, and (e) 1.0%. Points are coloured according to latitude, and the corresponding Pearson's correlation coefficient (r) and significance level (p) are shown in each panel. Significant positive correlations ($p < 0.001$) were observed at all supeFrsaturation levels.

https://doi.org/10.5194/egusphere-2026-3546
Preprint. Discussion started: 7 August 2026
© Author(s) 2026. CC BY 4.0 License.

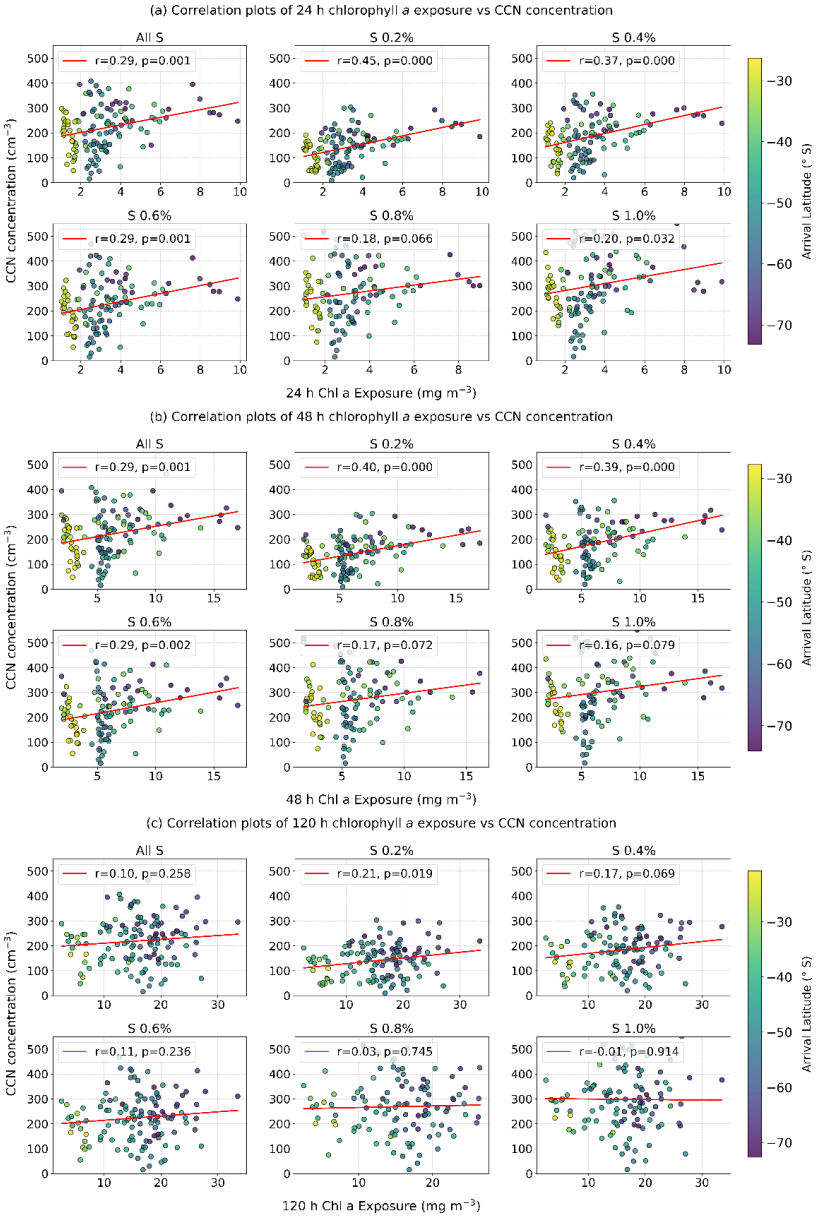

Figure 7: Scatter plots showing the relationship between CCN concentration and integrated chlorophyll a exposure along (a) 24 h, (b) 48 h, and (c) 120 h back trajectories for all supersaturation levels. Pearson's correlation coefficient (*r*) and corresponding *p-value* are shown in each panel. Positive correlations are strongest for the 24 h and 48 h exposure periods, particularly at lower supersaturation levels, whereas the correlations weaken substantially for the 120-h exposure period, indicating a stronger association

https://doi.org/10.5194/egusphere-2026-3546
Preprint. Discussion started: 7 August 2026
© Author(s) 2026. CC BY 4.0 License.

between recent exposure to biologically productive oceanic regions and CCN concentrations. Marker colours indicate the air-mass arrival latitude.

https://doi.org/10.5194/egusphere-2026-3546
Preprint. Discussion started: 7 August 2026
© Author(s) 2026. CC BY 4.0 License.

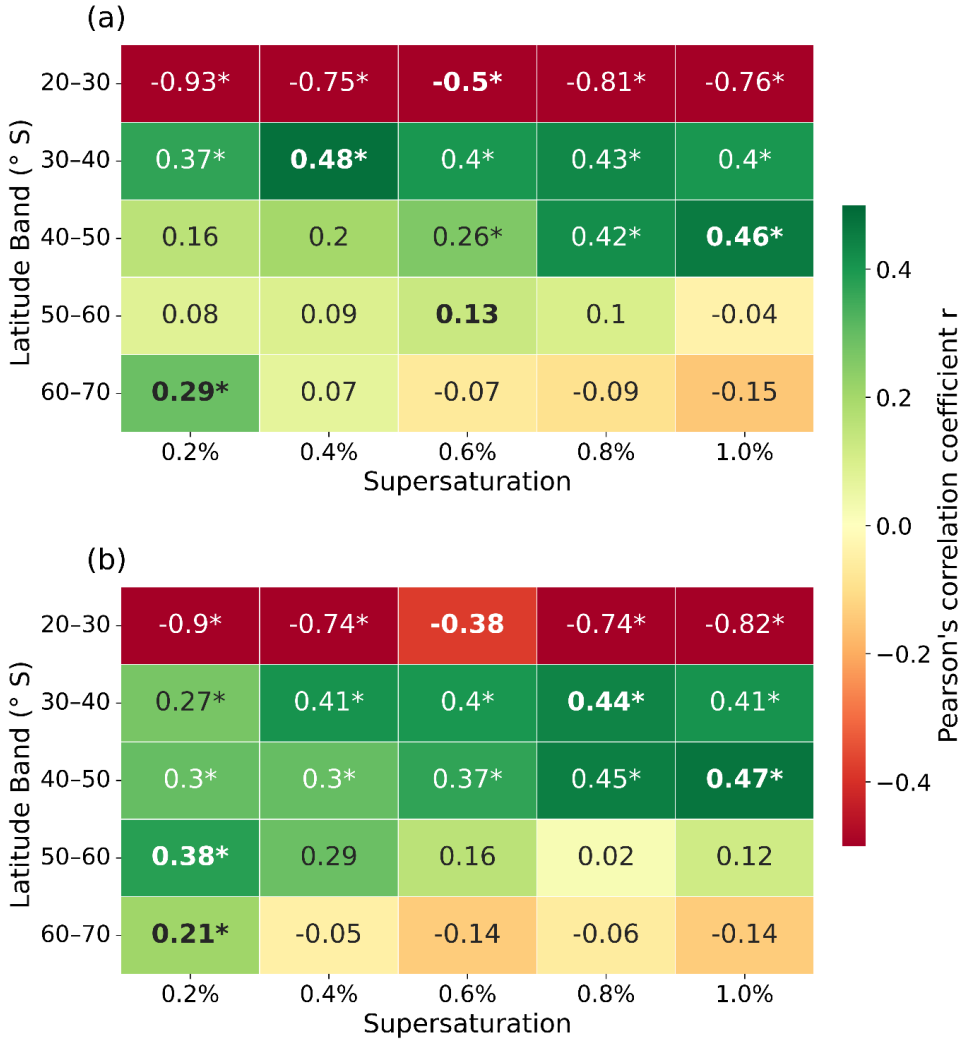

Figure 8: Heatmaps of Pearson's correlation coefficients (*r*) between chlorophyll a exposure and CCN concentrations across latitude bands and supersaturation levels for (a) 24 h and (b) 48 h exposure periods. Asterisks (*) indicate statistically significant correlations ($p < 0.05$). Positive correlation coefficients indicate that air masses passing over biologically productive waters were associated with higher CCN concentrations.